REPORT 198

KOMATIITE CHARACTERISTICS OF THE FISHER EAST NICKEL SULFIDE PROSPECTS: IMPLICATIONS FOR NICKEL PROSPECTIVITY IN THE NORTHEASTERN YILGARN CRATON

by LL Burley and SJ Barnes

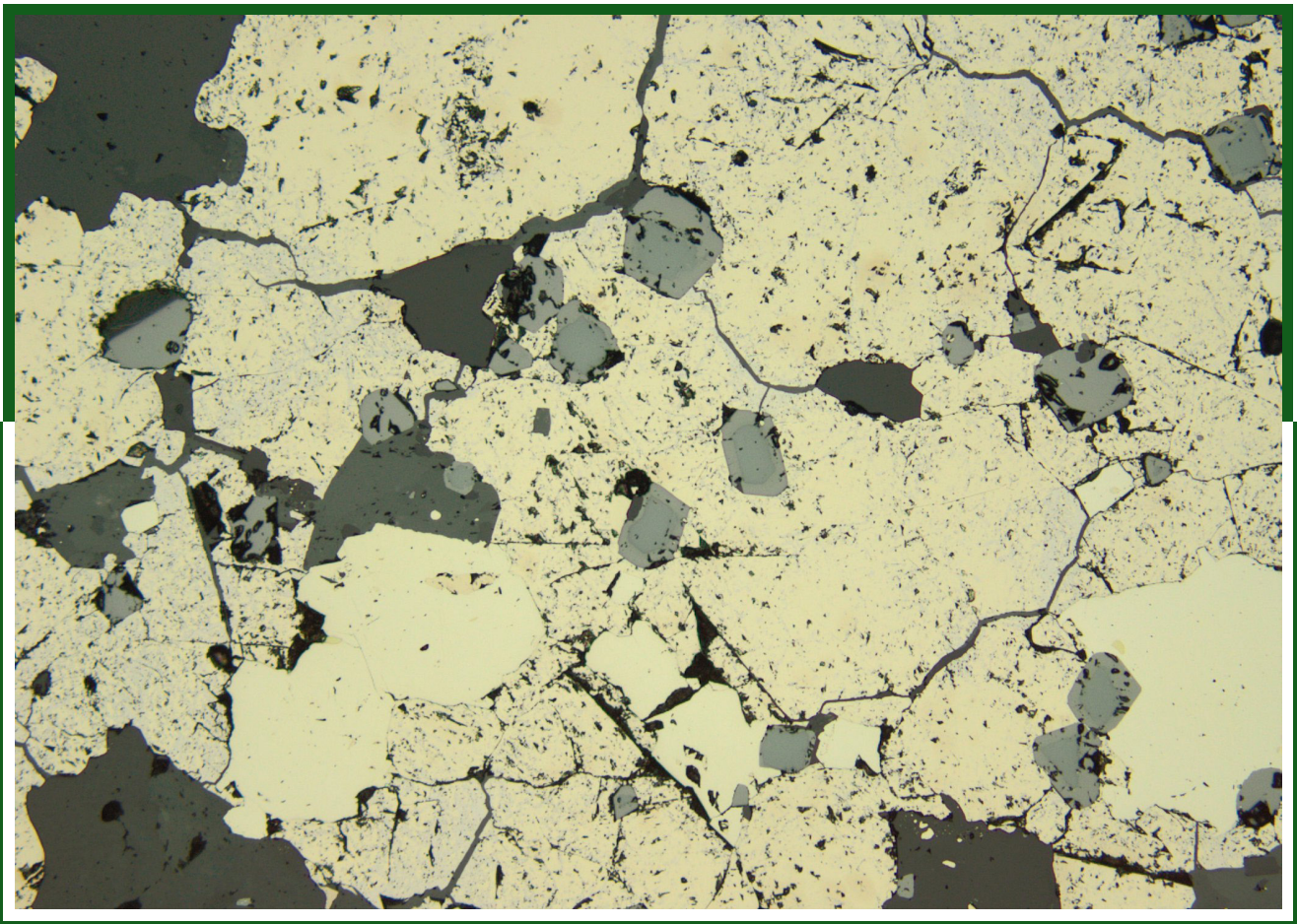

Government of Western Australia
Department of Mines, Industry Regulation and Safety

Geological Survey of Western Australia

Government of **Western Australia**
Department of **Mines, Industry Regulation and Safety**

REPORT 198

KOMATIITE CHARACTERISTICS OF THE FISHER EAST NICKEL SULFIDE PROSPECTS: IMPLICATIONS FOR NICKEL PROSPECTIVITY IN THE NORTHEASTERN YILGARN CRATON

by
LL Burley and SJ Barnes*

* CSIRO Mineral Resources, Technology Park, Kensington WA 6151

PERTH 2019

Geological Survey of Western Australia

MINISTER FOR MINES AND PETROLEUM
Hon Bill Johnston MLA

DIRECTOR GENERAL, DEPARTMENT OF MINES, INDUSTRY REGULATION AND SAFETY
David Smith

EXECUTIVE DIRECTOR, GEOLOGICAL SURVEY AND RESOURCE STRATEGY
Jeff Haworth

REFERENCE
The recommended reference for this publication is:
Burley, LL and Barnes, SJ 2019, Komatiite characteristics of the Fisher East nickel sulfide prospects: implications for nickel prospectivity in the northeastern Yilgarn Craton: Geological Survey of Western Australia, Report 198, 20p.

ISBN 978-1-74168-869-6
ISSN 1834-2280

A catalogue record for this book is available from the National Library of Australia

Grid references in this publication refer to the Geocentric Datum of Australia 1994 (GDA94). Locations mentioned in the text are referenced using Map Grid Australia (MGA) coordinates, Zone 51. All locations are quoted to at least the nearest 100 m.

Published 2019 by the Geological Survey of Western Australia
This Report is published in digital format (PDF) and is available online at <www.dmp.wa.gov.au/GSWApublications>.

Further details of geoscience publications are available from:
Information Centre
Department of Mines, Industry Regulation and Safety
100 Plain Street
EAST PERTH WESTERN AUSTRALIA 6004
Telephone: +61 8 9222 3459 Facsimile: +61 8 9222 3444
www.dmp.wa.gov.au/GSWApublications

Cover photograph: Reflected light image of massive sulfides with small chromite grains, being replaced by magnetite

Contents

Figures

Tables

Appendices

Available with the PDF online as an accompanying digital resource

Komatiite characteristics of the Fisher East nickel sulfide prospects: implications for nickel prospectivity in the northeastern Yilgarn Craton

by

LL Burley and SJ Barnes*

Abstract

Until recently, the Kurnalpi and Burtville Terranes of the eastern Yilgarn Craton have received little attention in terms of nickel sulfide exploration. However, recent discoveries of komatiite-hosted nickel sulfides in these terranes indicate them to be prospective, but underexplored. In this Report, we compare the lithostratigraphic, geochemical and mineralogical characteristics of komatiites with nickel sulfide mineralization at the newly discovered Fisher East prospects with those of the highly nickel-endowed Kalgoorlie Terrane to assess the potential of the Kurnalpi and Burtville Terranes for nickel mineralization. The komatiites at Fisher East are extensively deformed, pervasively altered to talc–carbonate assemblages, and primary textures are typically destroyed. Nonetheless, the ultramafic units can be differentiated into upper A-Zones (possibly originally spinifex textured) and lower B-Zones (olivine cumulates) on the basis of local relict igneous and secondary textures, hyperspectral data and geochemistry. B-Zones are typically much thicker than A-Zones and contain higher proportions of talc, MgO and Ni, with lower proportions of chlorite, Al_2O_3, TiO_2 and Zr. These characteristics, together with generally elevated Ni/Ti and Ni/Cr ratios suggest that the komatiites at Fisher East were erupted as high-energy channelized sheet flows favourable for developing olivine cumulate zones. Fisher East komatiites are Al-undepleted to weakly Al-enriched, indicating a slightly different composition to komatiites in the Kalgoorlie Terrane (mostly Al-undepleted) and southern Youanmi Terrane (e.g. Al-undepleted and Al-depleted komatiites of the Forrestania and Lake Johnston greenstone belts). Geochemical proxies such as Zr/Ti and La/Sm ratios indicate varying degrees of crustal contamination, which is favourable for the development of the sulfur saturations that are necessary for crystallization of sulfides. Although Fisher East komatiites are broadly more comparable to those of the Youanmi Terrane in terms of lithostratigraphy and age, they share similar characteristics to Kalgoorlie Terrane komatiites when it comes to proxies for mineralization, for example, thick cumulate zones indicating hot, turbulent lava flow channels, and evidence for crustal contamination. Further study of the Fisher East greenstone belt will assist future research into the prospectivity of the greenstone belts in the neighbouring Kurnalpi and Burtville Terranes.

KEYWORDS: Burtville Terrane, geochemistry, komatiites, Kurnalpi Terrane, nickel sulfides, Yilgarn Craton

Introduction

The vast majority of Australia's nickel sulfide resources are hosted in komatiites, ensuring their importance as exploration targets (Hoatson et al., 2006). Since the 1970s, the discovery rate of economic nickel deposits in the Yilgarn Craton has declined sharply (Hronsky and Schodde, 2006) and explorers have shifted their search to spaces that are 'blind' to traditional exploration methods, for example, by exploring at greater depths or in areas with thick regolith cover. However, recent advances in geochemical techniques have enabled explorers to better identify favourable host rocks (Barnes, 2013) and thereby identify mineral and chemical gradients towards nickel mineralization.

The Kalgoorlie Terrane in the Eastern Goldfields Superterrane (EGST), Yilgarn Craton, hosts the majority of the known komatiite-hosted nickel sulfide deposits in Western Australia, including the world-class Perseverance and Mount Keith deposits in the Agnew–Wiluna greenstone belt, and the type locality for this mineralization style, the Kambalda dome. Such unrivalled fertility has ensured ongoing exploration in the Kalgoorlie Terrane, yet recent discoveries in less mature ('greenfield') areas, such as along the boundary between the Kurnalpi and Burtville Terranes of the EGST, demonstrate the potential for new nickel provinces in other parts of Western Australia.

This study focuses on the newly discovered Fisher East prospects (Fig. 1), which have a current combined estimated resource of 4.2 Mt at 1.9% Ni, equivalent to ~78 kt of Ni metal (Rox Resources Limited, 2019). Here, we document the volcanogenic characteristics of the host komatiites at Fisher East, with an emphasis on the primary magmatic processes that control nickel mineralization, and compare them with those of well-characterized Ni-bearing komatiites from the Kambalda and Agnew–Wiluna nickel camps.

Komatiites: physical and chemical properties

Komatiites are defined as volcanic or subvolcanic rocks derived from melts with liquid compositions >18 wt% MgO

* CSIRO Mineral Resources, Technology Park, Kensington WA 6151

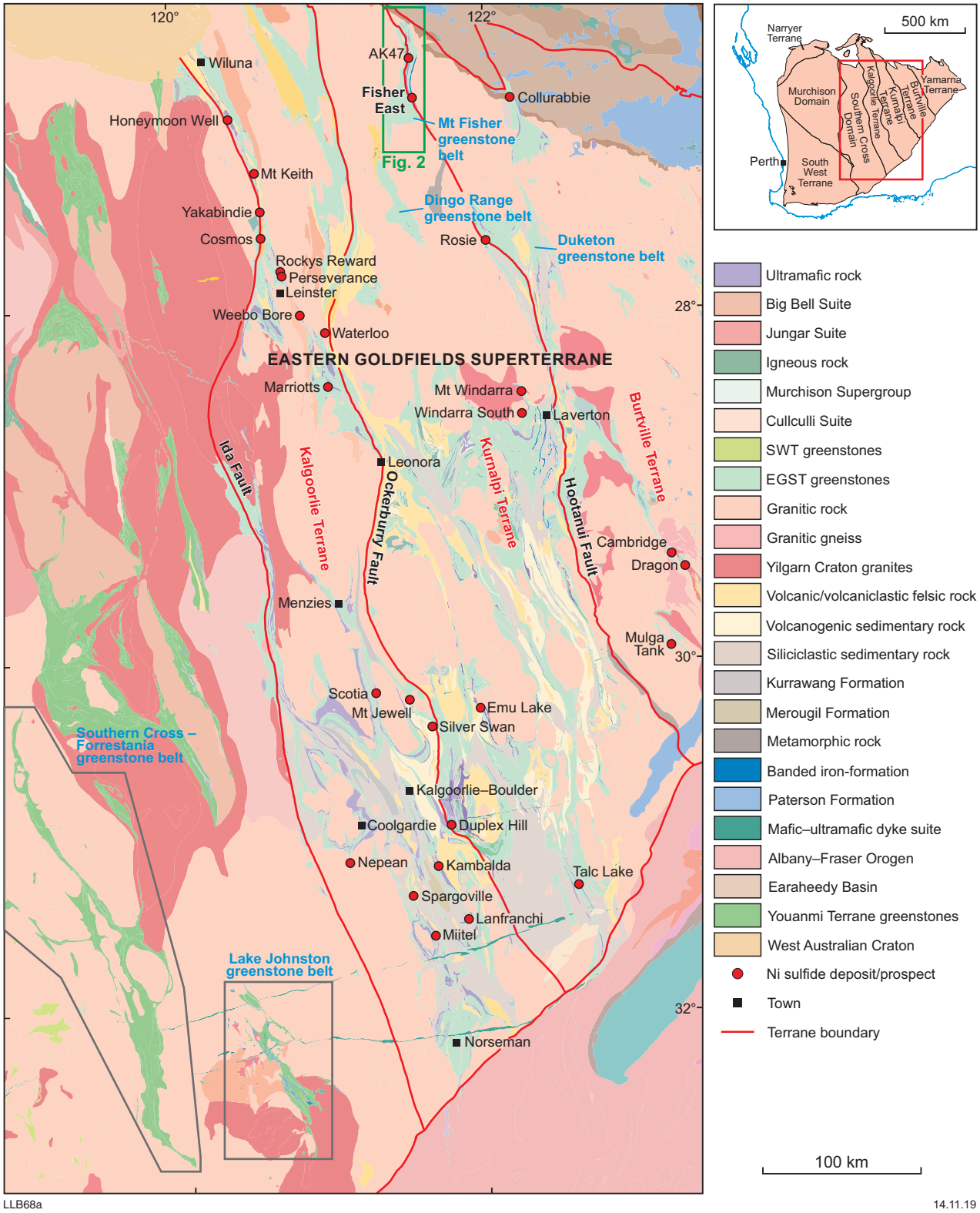

Figure 1. **Generalized bedrock geology (Martin et al., 2016) of the Eastern Goldfields Superterrane showing selected nickel deposits and prospects. Terrane boundaries are from Martin et al. (2017). Abbreviations: EGST, Eastern Goldfields Superterrane; SWT, South West Terrane**

(Arndt et al., 2008). Their geochemical and mineralogical compositions reflect anomalously high mantle temperatures that were likely common during the Archean, the age of almost all known examples of komatiites (e.g. Arndt et al., 2008; Herzberg et al., 2010). Many komatiites show internal differentiation into two main zones, an upper olivine spinifex-textured zone and a lower olivine cumulate zone, which are widely referred to as A- and B-Zones, respectively (Hill et al., 1988). Olivine spinifex textures are typically formed by relatively rapid in situ crystallization of olivine, usually at the top of a flow, whereas olivine cumulates are formed by slower crystallization of olivine, with crystals accumulating and settling at the base of a flow or sill (Hill et al., 1988). Cumulates can be divided into orthocumulates, mesocumulates and adcumulates on the basis of the tightness of their crystal packing, that is, how much liquid was trapped between the phenocrysts (Wager et al., 1960).

Primary mineral assemblages in komatiites are always altered to some degree (Barnes, 2006; Arndt et al., 2008). Mineral alteration assemblages vary according to factors including the bulk composition of the original lava, metamorphic temperature–pressure conditions, or interaction with metamorphic or hydrothermal fluids (Gole et al., 1987; Barnes, 2006; Arndt et al., 2008; Table 1). Hence, it is important to base geochemical identification of komatiites on the contents of elements such as Si, Cr, Al, Ti, Fe, Ni and Mg — initial quantities of which are usually retained in komatiites — and incompatible trace elements such as rare earth elements (REE) and high field strength elements (HFSE) (Hill et al., 1988; Barnes et al., 2004; Barnes, 2006; Table 1). This is important because mantle source information and exploration vectoring tools can be derived from these elements. For example:

- MgO/FeO ratios are used to estimate primary komatiite liquid and olivine compositions (Barnes et al., 2004; Barnes, 2006).
- Al_2O_3/TiO_2 ratios are used to classify komatiites as Al-depleted, Al-undepleted or Al-enriched, which may inform assumptions and interpretations regarding their mantle source compositions and geodynamic processes (Nesbitt et al., 1979; Sproule et al., 2002; Wilson, 2003).
- Incompatible trace element ratios (e.g. Zr/TiO_2, La/Sm, Th/Nb) are used to assess the extent to which magmas have assimilated crustal materials (e.g. Perring et al., 1996; Barnes et al., 2004; Barnes, 2006).
- Ni/Ti and Ni/Cr ratios are used to distinguish magma pathways favourable for nickel sulfide mineralization, such as olivine-adcumulate-rich channels, from low-energy depositional environments like channel flanks, which are typically unfavourable for mineralization (e.g. Barnes et al., 2004).

Barnes et al. (2004) described five major volcanic facies that are common constituents of komatiitic flow fields (Table 2):

- thin differentiated flows (TDF)
- compound sheet flows with internal pathways (CSF)
- dunitic compound sheet flows (DCSF)
- dunitic sheet flows (DSF)
- layered lava lakes or sills (LLLS).

Table 1. General characteristics of A- and B-Zone komatiites, summarized from Barnes (2006)

	A-Zone komatiites	*B-Zone komatiites*
Primary igneous textures	Spinifex textures	Cumulate textures (ad-, meso- and orthocumulates)
Primary mineralogy	Olivine and/or pyroxene	Olivine
Geochemical characteristics	Typically, 20–32 wt% MgO Higher Al_2O_3, TiO_2 and SiO_2	Typically >32 wt% MgO Lower Al_2O_3, TiO_2 and SiO_2
Typical mineralogy in CO_2-rich conditions — greenschist facies	Tremolite–chlorite–dolomite	Quartz–magnesite–dolomite–chlorite **or** talc–chlorite–dolomite–magnesite (ortho- and mesocumulates) **or** talc–magnesite (adcumulates)

Table 2. Descriptions of komatiite volcanic facies (Barnes et al., 2004)

Facies	*Description*	*Type examples*
Thin differentiated flows (TDF)	Multiple compound spinifex-textured flows; generally less than 10 m thick, with internal differentiation into spinifex and cumulate zones	Munro Township (Pyke et al., 1973)
Compound sheet flows with internal pathways (CSF)	Compound thick cumulate-rich flows, with central olivine-rich lava pathways flanked by multiple thin differentiated units, from tens of metres to ~200 m maximum thickness	Silver Lake Member at Kambalda (Lesher et al., 1984)
Dunitic compound sheet flows (DCSF)	Thick olivine-rich sheeted units with central lenticular bodies of olivine adcumulates, up to several hundred metres thick and 2 km wide, flanked by laterally extensive thinner orthocumulate-dominated sequences with minor spinifex. CSF and DCSF correspond to 'Flood Flow Facies' of Hill et al. (1995).	Perseverance and Mount Keith (Hill et al., 1995)
Dunitic sheet flows (DSF)	Thick, laterally extensive, unfractionated sheet-like bodies of olivine adcumulates and mesocumulates, in some cases laterally equivalent to layered lava lake bodies	Southern section of the Walter Williams Formation (Gole and Hill, 1990; Hill et al., 1995)
Layered lava lakes and/or sills (LLLS)	Thick, sheeted bodies of olivine mesocumulates and adcumulates with lateral extents of tens of kilometres, with fractionated upper zones including pyroxenites and gabbros, up to several hundred metres in total thickness	Kurrajong Formation (Gole and Hill, 1990; Hill et al., 1995)

Of these, only DCFS and CSF facies are known to host nickel sulfide mineralization. Both of these facies represent high-flow magma pathways characterized by olivine cumulates and can be identified by their elevated Ni/Ti and Ni/Cr ratios and low Cr contents (Barnes et al., 2004).

The most widely accepted model for formation of komatiite-hosted nickel sulfide mineralization is that of Lesher (1989), who proposed that komatiitic magmas were initially sulfur undersaturated, and that saturation was achieved during emplacement by assimilation of sulfur-rich sediments and continental crust. Hence, geochemical proxies for crustal contamination can be used as indicators for nickel sulfide mineralization. The most comprehensive classification for komatiite-hosted Ni–Cu–PGE (platinum group elements) deposits is that of Lesher and Keays (2002), who proposed five deposit types based on their style of mineralization (summarized in Table 3).

Komatiites of the Yilgarn Craton

In the Yilgarn Craton, komatiites that host nickel sulfides vary in age, composition and stratigraphic setting. Komatiites in the Forrestania and Lake Johnston greenstone belts of the Youanmi Terrane erupted at c. 2.9 Ga and have both Al-depleted and Al-undepleted compositions (Perring et al., 1996). They were deposited in a supracrustal sequence dominated by metabasaltic and metasedimentary rocks, including numerous sequences of banded iron-formation (BIF) (Barnes and Fiorentini, 2012). Interestingly, the Forrestania and Lake Johnston greenstone belts are the only areas worldwide where Al-depleted komatiites are known to host significant nickel sulfide mineralization (Barnes and Fiorentini, 2012). In contrast, komatiites in the Kalgoorlie Terrane erupted at c. 2.7 Ga (Nelson, 1997) and are typically associated with felsic volcanic rocks or tholeiitic basalts (Barnes and Fiorentini, 2012); the majority of them have Al-undepleted compositions (Barnes, 2006). Little is known about komatiites in the Kurnalpi, Burtville and Yamarna Terranes, although they are thought to be of c. 2.8 Ga age (Kositcin et al., 2008; Miller, 2010), slightly older than those in the Kalgoorlie Terrane. Studies of the Windarra nickel deposits in the Kurnalpi Terrane indicate that komatiites there are associated with mafic and ultramafic rocks (Schumulian, 1984). Exploration models need to accommodate these key differences in age, chemistry and lithological associations of komatiites in the various terranes of the Yilgarn Craton.

Regional geological setting

The Fisher East nickel prospects are in the Mount Fisher greenstone belt along the boundary between the Kurnalpi and Burtville Terranes in the northeast of the EGST (Fig. 1). Opinions are divided on the appropriate geodynamic model for the EGST; recent studies have proposed both a tectonic mosaic of juxtaposed arc–back-arc terranes model (Barley et al., 1989; Krapez and Barley, 2008; Czarnota et al., 2008, 2010; Korsch et al., 2011) and a vertical tectonic, plume-driven model (Barnes et al., 2012; Barnes and Van Kranendonk, 2014; Witt et al., 2018). Numerous fault systems, such as the Ida, Ockerburry and Hootanui systems, mark the boundaries between the various domains and terranes of the EGST (Swager et al., 1992; Swager, 1997; Czarnota et al., 2008).

The majority of the greenstone belts in the EGST were formed between c. 2.72 and 2.65 Ga (Czarnota et al., 2008; Said et al., 2012); however, those in the Burtville Terrane have yielded U–Pb zircon dates between c. 2.96 and 2.77 Ga (Kositcin et al., 2008; Geological Survey of Western Australia [GSWA], 2009). Although the geodynamic history of the Burtville Terrane and its relationship to the neighbouring Kurnalpi and Yamarna Terranes are poorly understood, the majority of authors agree that the Burtville Terrane likely formed during an earlier event than the Kurnalpi and Kalgoorlie Terranes (Standing, 2008; Pawley et al., 2009; Begg et al., 2010) and shows a greater resemblance to the 2.9–2.7 Ga Murchison Domain of the Youanmi Terrane (Pawley et al., 2009).

The supracrustal sequence in the surrounds of the Mount Fisher region is dominated by BIF, ultramafic–mafic volcanic sequences and fine-grained volcanogenic sedimentary rocks; U–Pb zircon geochronology constrains most of this sequence to older than c. 2.72 Ga, and potentially as old as c. 2.8 Ga (Cassidy et al., 2006; Kositcin et al., 2008).

Methods

The analytical components of this study were conducted exclusively on drillcore, as outcrop in the region is rare. Geological logging, thin-section petrography, infrared spectrometry, X-ray fluorescence micromapping and whole-rock geochemistry were conducted on komatiites and the enveloping supracrustal sequence.

Geological logging and sampling of diamond drillcore

Cores from 10 drillholes from the Fisher East prospects (provided by Rox Resources) were selected for geological logging, geochemical analysis and petrographic characterization (Fig. 2). The sampled intervals were from 20 m beneath the stratigraphic footwall of ultramafic rocks to the top of ultramafic units in the hangingwall. The drillholes were selected from four prospects in the Fisher East area: Camelwood, Cannonball, Musket and Sabre (Fig. 2b). Holes were chosen that either intercepted mineralization or were drilled on the flanks of mineralized zones. An extra drillhole (MFED001; Fig. 2b), which was drilled under the GSWA Exploration Incentive Scheme, was logged and scanned by the HyLogger instrument, but was not sampled for geochemistry.

Representative samples were collected from most of the lithologies intersected by the drillholes. Polished thin sections were prepared from 24 of these samples for transmitted and reflected light petrographic analysis to determine mineral assemblages, textures and structures.

Whole-rock geochemistry

A total of 105 samples were collected for whole-rock geochemical analysis to allow comparison of the bulk compositions and chemical variations among the ultramafic units. Representative samples were selected from throughout the stratigraphic sequence of each

Table 3. Classification scheme for komatiite-hosted nickel sulfide systems (after Lesher and Keays, 2002). Abbreviation: MSS, monosulfide solid solution

Origin	*Magmatic*						*Hydrothermal–metamorphic*		*Tectonic*
Type	*I* *Basal/footwall*		*II* *Stratabound internal*			*III* *Reef*	*IV*		*V*
Subtype	*Ia* *Stratiform*	*Ib* *Footwall vein*	*IIa* *Blebby*	*IIb* *Interstitial*	*IIc* *Cloudy*	*Stratiform*	*IVa* *Metasediment*	*IVb* *Vein*	*Offset*
Sulfide distribution	At or near the bases of komatiitic peridotite or komatiitic dunite units	Veins or stringers in host or wallrocks associated with Type Ia mineralization	Coarse disseminations within komatiitic peridotite or dunite units	Fine disseminations within komatiitic peridotite or dunite units	Very fine disseminations within komatiitic peridotite or dunite units	At or near contact between lower cumulate zones and upper gabbro zones within strongly differentiated units	Layers in sulfidic metasediments associated with Type I mineralization	Veins in wallrocks associated with Type I mineralization	Faults and shear zones within host- or wallrocks associated with Type I mineralization
Sulfide textures	Massive, net-textured, disseminated; sometimes xenolith- or xenomelt-bearing	Massive	Blebby	Intercumulus, interstitial or lobate	Intercumulus, interstitial	Disseminated; rarely net-textured	Layered, banded, laminated	Massive to disseminated; typically associated with quartz and/or carbonate	Brecciated, typically heterolithic; durchbewegung
Ore tenor	Typically moderate–low; slightly fractionated	Variable; commonly enriched in Cu–PPGE relative to associated contact ores	Moderately high; relatively unfractionated	Typically high; relatively unfractionated	Variable (high to low)	Typically high; relatively fractionated	Variable; commonly depleted in Cr and Ir relative to associated magmatic ores	Variable; commonly depleted in Cr and Ir relative to associated magmatic ores	Variable; commonly depleted in Cr, Pt and Au relative to magmatic ores
Timing and paragenesis	Early magmatic; segregated prior to or during emplacement	Early or late magmatic; injected during initial emplacement or formed via fractional crystallization of MSS	Intermediate magmatic; segregated during crystallization of cumulate host rock	Intermediate magmatic; segregated during crystallization of host rock	Late magmatic but metamorphically modified; segregated during crystallization of cumulate host rock	Late magmatic; segregated during final stages of crystallization of host rock	Late magmatic or synmetamorphic	Synmetamorphic; mobilized in hydrothermal fluids	Syntectonic; mobilized from massive or net-textured sulfides
Examples (see table 2 of Lesher and Keays, 2002)	Alexo, Kambalda, Katinniq, Langmuir, Windarra	Kambalda, Alexo, Katinniq	Damba-Silwane, Otter shoot (Kambalda)	Mt Keith, Dumont, Perseverance Main	Katinniq, Perseverance Main	Delta, Romeo II, Fred's Flow, Boston Creek Unit	Jan shoot (Kambalda), Langmuir, Redstone, Thompson	Kambalda, Langmuir, Donaldson West	Thompson, Nepean, Perseverance 1A, Redross, Redstone, Trojan, Windarra

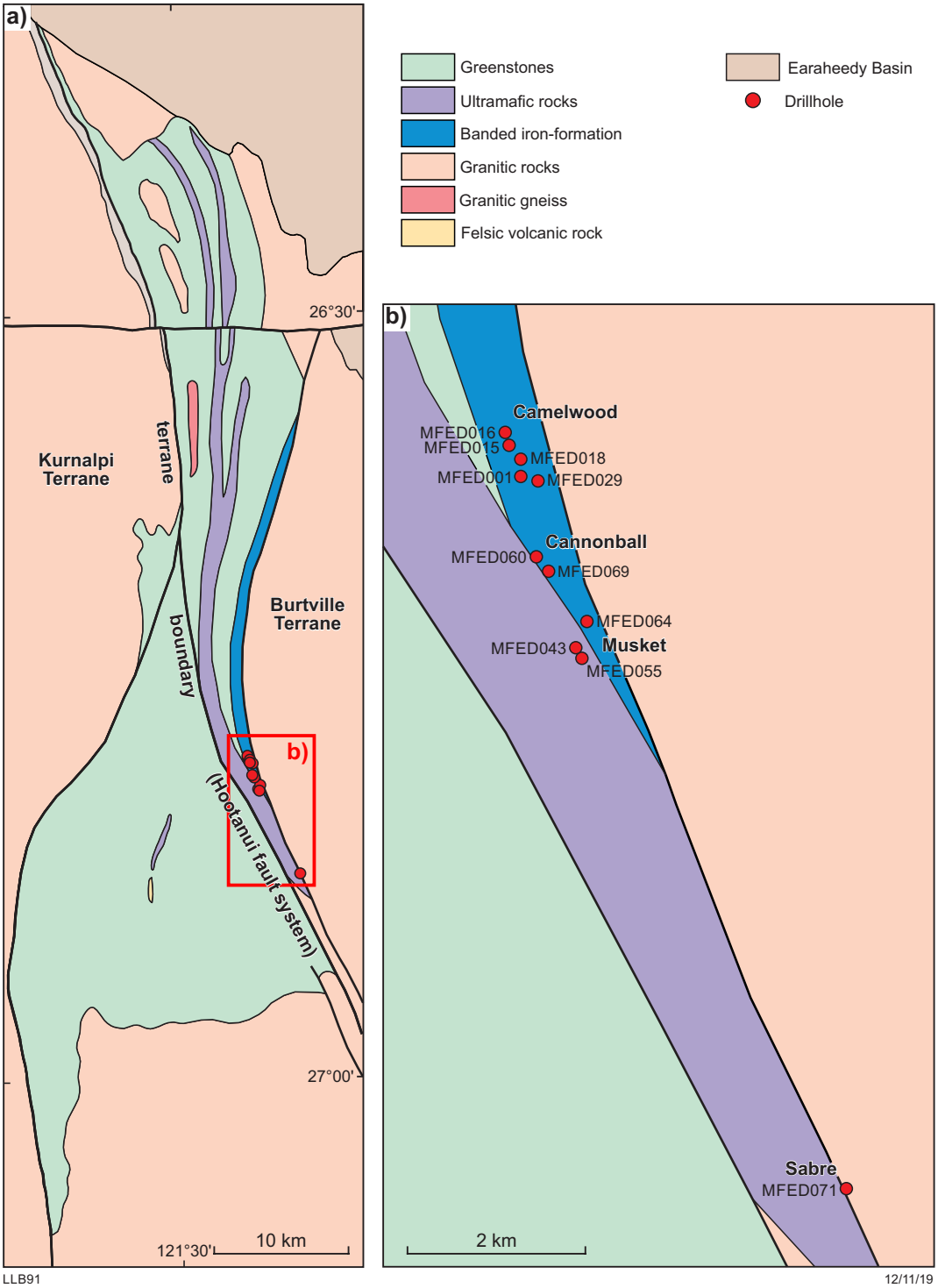

Figure 2. **Generalized bedrock geological maps of the Mount Fisher greenstone belt showing locations of drillcore used in this study: a) regional map; b) detailed map over Fisher East prospects. Geology and structural lines from 1:500 000 interpreted bedrock geology of Western Australia (Martin et al., 2016). Terrane boundary after Cassidy et al. (2006)**

core, with care taken to avoid veins and xenoliths of country rock. Major element oxides, trace elements and REE were analysed by Genalysis Intertek Laboratories in Perth, Western Australia (analytical techniques provided in Appendix 1). Platinum, Pd and Au contents were determined by fire assay for samples of felsic, metasedimentary and ultramafic rocks within 2 m of the basal ultramafic contact. All geochemical data reported (excluding Ni and Cu) have been amended for volatile and sulfide contents.

Portable X-ray fluorescence spectrometry

A total of 849 non-destructive geochemical measurements of drillcore was acquired by portable X-ray fluorescence (pXRF) spectrometry, including the 105 samples analysed by traditional whole-rock chemistry methods. An Olympus InnovX handheld pXRF analyser was used in 'soil mode' to collect analyses at about 1 m intervals within the ultramafic sequences and at about 5 m intervals in other parts of the core. Instrument performance was calibrated before and after each batch of 15 core analyses by using a steel plate and pulverized reference material (standard) contained in a thin plastic bag (see Le Vaillant et al., 2014). Temporal instrument drift and precision were measured and assessed using the methods of Le Vaillant et al. (2014). All pXRF data acquired for this study were corrected for the effect of measuring standards through plastic bags (using attenuation factors from Le Vaillant et al., 2014). Although several other elements were measured, only Ni, Ti, Cr and Zr data were used in this study. A comparison of the pXRF and traditional whole-rock geochemical data is presented in Appendix 2; a more detailed comparison is provided by Burley et al. (2017). Standard compositions, plastic attenuation factors, graphs of instrument drift, and instrument and sample precision are presented in Appendix 3.

Hyperspectral logging

Ten of the eleven diamond drillcores (excluding MFED015) were continuously scanned using GSWA's HyLogger-3, employing methodology described by Hancock and Huntington (2010) and Hancock et al. (2013). Reflectance spectra were collected over the visible to near infrared (380–1000 nm), short-wave infrared (1000–2500 nm) and thermal infrared (6000–14 500 nm) wavelength ranges to determine the abundance and composition of a range of common rock-forming minerals (Hancock et al., 2013). High-resolution (0.1 mm pixel) digital colour photographs of core were concurrently obtained using a built-in line-scan camera. The reflectance spectra were automatically resampled to 8 nm spectral resolution and 8 mm spatial resolution by The Spectral Geologist software (TSG; www.thespectralgeologist.com).

Raw (resampled) HyLogger-3 spectral data were processed using The Spectral Assistant (TSA) algorithm built in to the TSG HotCore software (Huntington et al., 1997). TSA compares drillcore spectra with a reference library of typical mineral spectra to identify best matched minerals, and estimates their relative proportions and fitting errors (Berman et al., 1999). These automated mineral identifications were validated to filter out obvious erroneous interpretations by manually refining the TSA matching scalars (uTSAV, uTSAS and uTSAT) and testing these using additional scalars in TSG (e.g. Cudahy et al., 2008; Laukamp et al., 2010, 2012; Sonntag et al., 2012).

TORNADO XRF mineral chemistry maps

Element distribution maps were obtained for selected quarter-core, half-core and thin section samples by using a Bruker M4 TORNADO micro-XRF spectrometer at the CSIRO Advanced Resource Characterisation Facility in Kensington, Western Australia. The spectrometer was equipped with a rhodium X-ray tube operating at 50 kV and 500 nA without filters, and an XFlash silicon drift X-ray detector (Bruker Corporation, 2015). Each sample was line-scanned with a nominal 25 micron beam over a period ranging between two and four hours. Bruker M4 TORNADO software was used to produce false colour-coded multi-element maps depicting spatial variations in element concentrations that highlight textural variations that may not be visible in hand samples. The element distribution maps obtained and GSWA sample numbers from which they were derived are provided in Appendix 4.

Results

Local lithostratigraphy

Because Archean rocks rarely crop out in the Fisher East region, lithostratigraphic interpretations rely heavily on drillhole data, the majority of which are close to nickel sulfide deposits. The Fisher East stratigraphy consists of a basal sequence of felsic volcanic, volcaniclastic metasedimentary rocks and BIF, overlain by komatiites that are typically around 25 m thick, but can be up to ~90 m thick. The komatiites are locally overlain by either a metapelitic sequence (BIF, shale and sulfidic chert) or a basaltic sequence (Fig. 3). The supracrustal sequence is locally intruded by quartz porphyries, lamprophyres and felsic dykes. The komatiites have a maximum age of c. 2940 Ma, constrained by zircon U–Pb dates from underlying felsic volcanic and volcaniclastic rocks, and a minimum age of c. 2840 Ma based on zircon U–Pb dates from intermediate volcaniclastic rocks in the hangingwall (Mole et al., 2016). The komatiitic and metasedimentary units show strong foliations that are subparallel to lithological contacts and the entire sequence is locally overturned.

The western (interpreted footwall) contact of the komatiite shows evidence of thermal erosion and assimilation of underlying rocks, with rounded quartz clasts (interpreted detrital origin) within komatiites immediately above the footwall metasedimentary rocks (Fig. 4) and xenoliths of metasedimentary rock locally within massive sulfide zones (Fig. 5). Mingling of komatiites and metasedimentary rocks is apparent in drillhole MFED069 (Fig. 6) and soft sediment deformation is evident in drillhole MFED043 (Fig. 7).

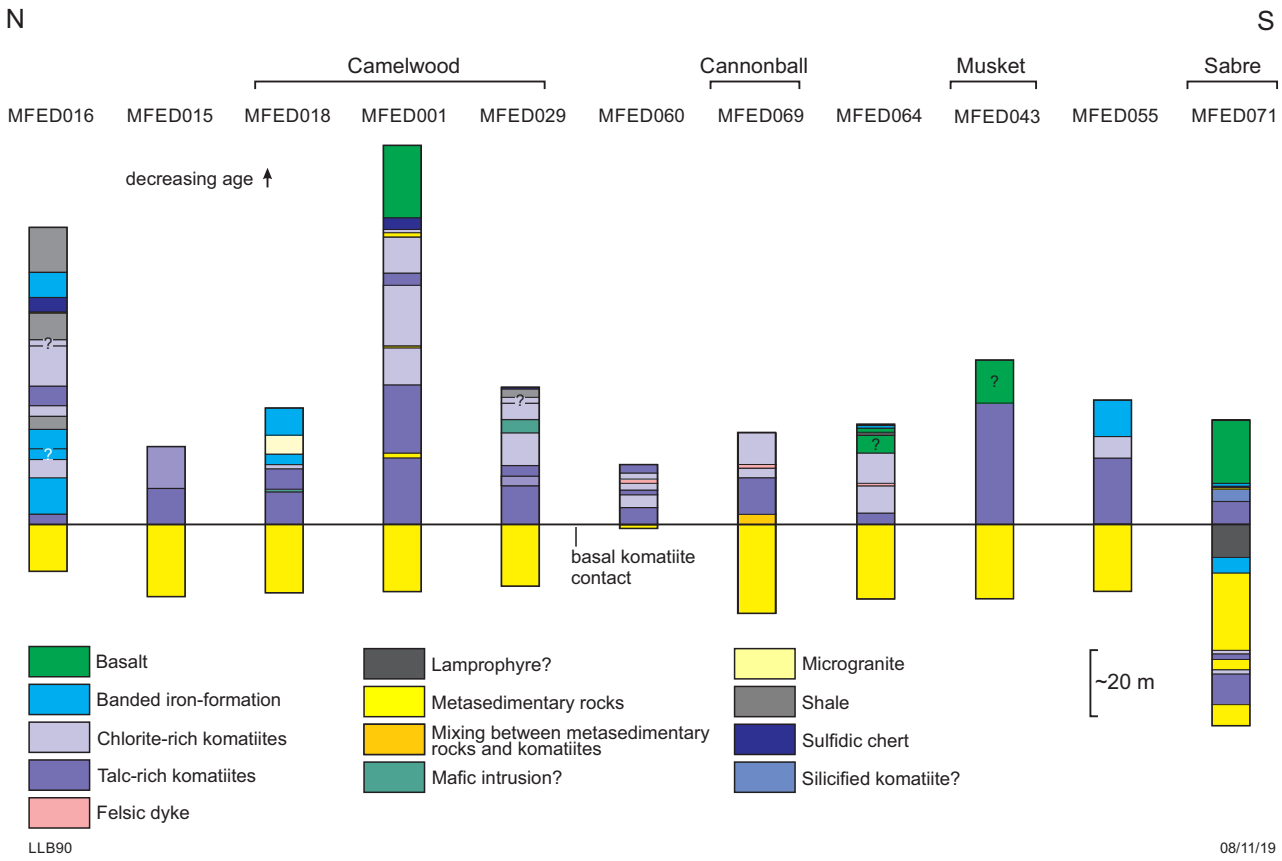

Figure 3. **Stratigraphy at Fisher East as defined by core logging and geochemistry. Note the arbitrary horizontal scale (e.g. drillhole MFED071 is about 7 km south of the Musket prospect). Datum for the basal komatiite contacts is 0 m above sea level. This model does not consider topographic changes or structural complexity**

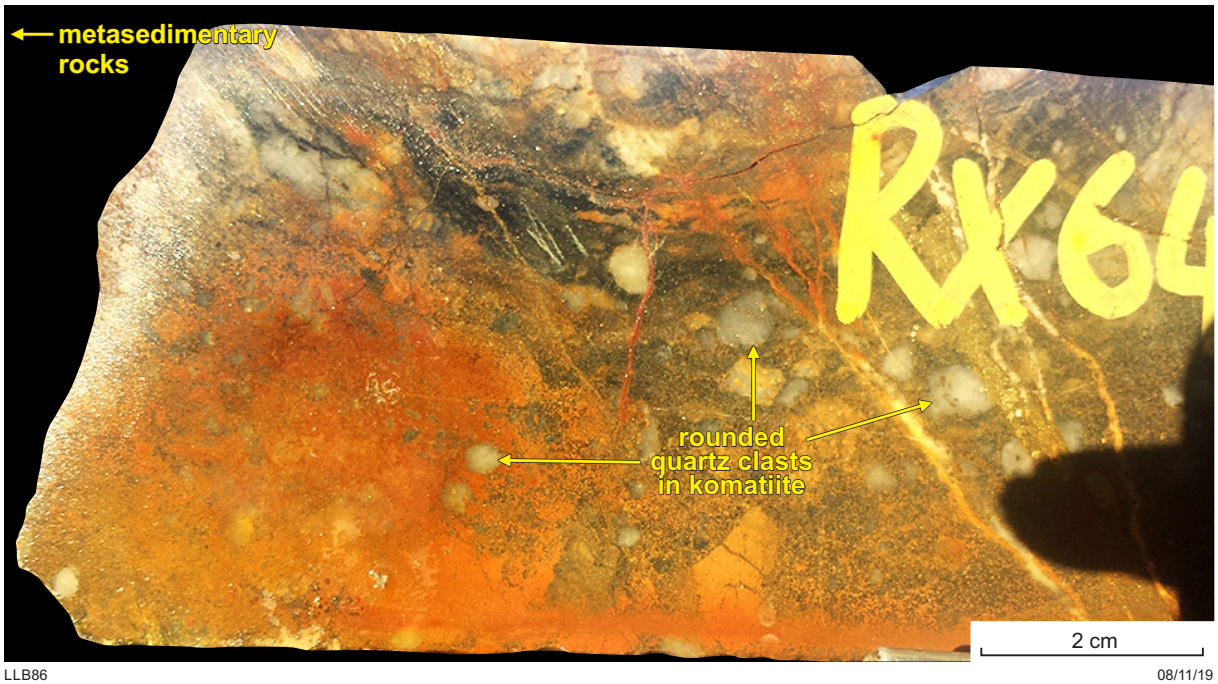

Figure 4. **Photo showing inclusions of rounded detrital quartz clasts within komatiite close to its lithological contact with felsic metasedimentary rocks from which they were likely assimilated. Drillhole MFED016 ~208 m**

Figure 5. Core photo showing a xenolith of felsic metasedimentary rock (red circle), presumably 'ripped up' during deposition of massive komatiite-hosted sulfides. This xenolith indicates assimilation/interaction between country rocks and later komatiitic units. Drillhole MFED043 ~305.05 m

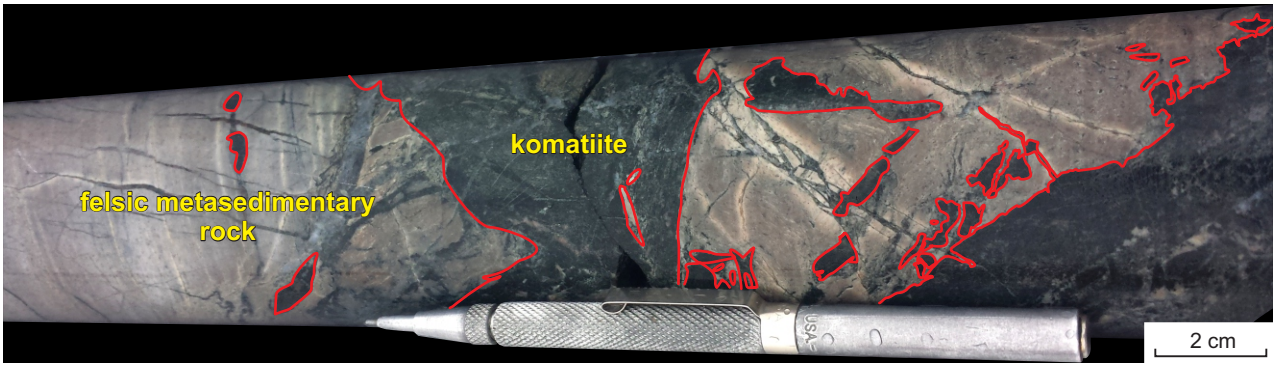

Figure 6. Core photo showing interaction between felsic metasedimentary rock and komatiitic material (outlined in red). Drillhole MFED069 ~243 m

Figure 7. Core photo showing soft sediment deformation at a contact between felsic metasedimentary rock and massive sulfides (hosted in talc-rich komatiite). Drillhole MFED043 ~305 m

BIF is commonly in contact with komatiites in inferred flanking environments, but the absence of BIF in interpreted channels suggests assimilation of these rocks by komatiites (Fig. 3). The eastern (interpreted hangingwall) contact between the komatiite and the overlying metasedimentary or basaltic rocks is sharper than the basal contact and, where preserved, shows no primary magmatic interaction with the adjacent rocks (e.g. Fig. 8). Hence, the upper contact is likely a conformable stratigraphic contact, or possibly a fault contact.

Deformation is evident in each of the Fisher East prospects, but the extent of displacement of country rocks is uncertain. For example, drillholes MFED016 and MFED071 both intersect multiple komatiite units that have sharp bounding contacts with country rocks and show no evidence of magmatic alteration or assimilation of country rocks (Fig. 3). It is likely that these intersections represent structural repetition of one or more komatiite units.

Texture, mineralogy and geochemistry of komatiites

The komatiites at Fisher East are intensely altered to talc–carbonate–chlorite assemblages and the majority of them are strongly foliated. Consequently, primary textures (e.g. spinifex texture, crystal boundaries in olivine cumulate zones) are typically destroyed and strongly overprinted by tectonometamorphic fabrics (e.g. Figs 9, 10). However, the komatiites appear to retain broad chlorite-rich and talc-rich zones with distinct differences in texture, mineralogy and geochemistry, likely related to primary zonation within komatiite flow profiles. Differentiation between these two alteration variants might assist in interpreting volcanogenic processes and understanding magmatic conditions relevant to nickel sulfide mineralization at Fisher East.

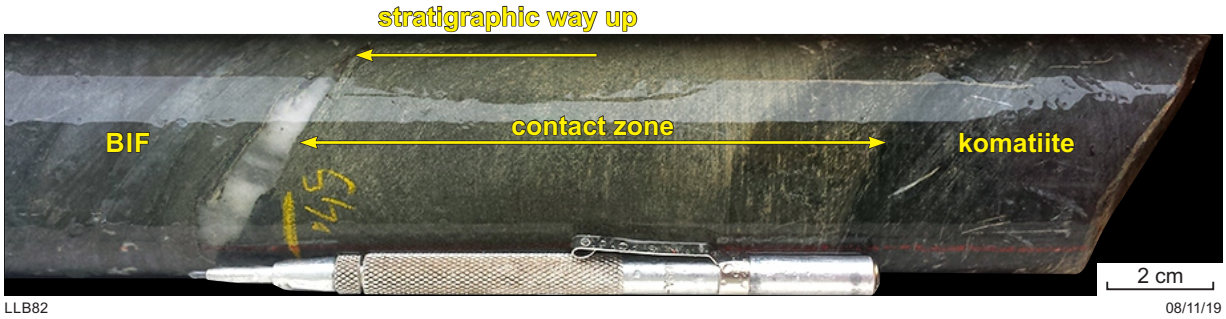

Figure 8. Core photo showing hangingwall contact between komatiite and BIF. Drillhole MFED055 ~306.5 m

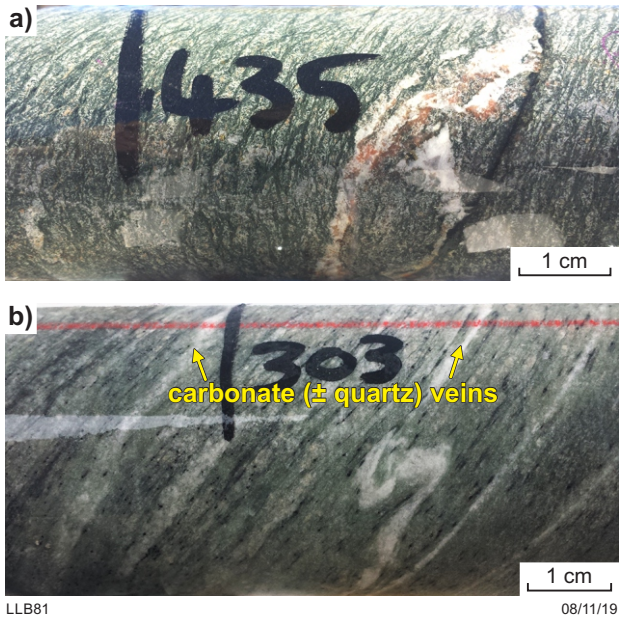

Figure 9. Core photos of chlorite-rich komatiites at drillholes: a) MFED029 ~435m; b) MFED055 ~303 m

Chlorite-rich komatiites at Fisher East are typically finer grained than talc-rich komatiites and have chlorite-rich matrixes with pervasive carbonate(±quartz) veining (Fig. 9). Talc-rich komatiites, on the other hand, have talc-rich matrixes with carbonate pseudomorphing primary phenocrysts (most likely olivine, e.g. Fig. 10). HyLogger short-wave infrared hyperspectral analysis confirmed that the chlorite-rich komatiites are dominated by chlorite, with lesser amounts of talc; thermal infrared hyperspectral analysis indicated trace amounts of amphibole, plagioclase and quartz (Appendix 2). Short-wave infrared analysis showed that the talc-rich komatiites contain predominantly talc, with lesser amounts of carbonate and chlorite, and thermal infrared hyperspectral analysis indicated trace amounts of silica and mica. Thus, the talc-rich and chlorite-rich komatiite samples exhibited clear compositional differences; the chlorite-rich komatiites contain higher concentrations of Al_2O_3, TiO_2 and Zr, whereas the talc-rich komatiites contain significantly higher concentrations of MgO and Ni (Table 4). Nickel sulfides at Fisher East are more commonly associated with the thicker zones of talc-rich alteration in komatiite, rather than the chlorite-rich zones.

Komatiites at Fisher East have Al_2O_3/TiO_2 ratios of ~10 to 37 (average ~25) and plot immediately below chondritic mantle compositions on Al_2O_3–TiO_2 crossplots (Fig. 11), hence indicating that they have Al-undepleted or weakly Al-enriched compositions. Their REE patterns are most similar to those of Al-undepleted komatiites (Fig. 12). Ratios of incompatible trace elements, such as La/Sm and TiO_2/Zr ratios, suggest variable amounts of crustal contamination of komatiitic melts during their emplacement (Fig. 13).

Figure 14 shows the typical range of Ni/Ti and Ni/Cr ratios for komatiite volcanic facies subdivisions. These diagrams enclose 80% of data points from four volcanic facies from a global komatiite database (Barnes and Fiorentini, 2012). In addition, the Ni/Ti vs Ni/Cr ratios can be used to discriminate komatiitic basalts from other cumulate-textured rocks (Le Vaillant et al., 2016). Moreover, Ni, Ti and Cr detected by pXRF can be used to discriminate volcanic facies and rock types when major element chemistry is not available (e.g. Le Vaillant et al., 2014; Burley et al., 2017). For our drillhole samples from Fisher East, the Ni/Ti and Ni/Cr ratios we determined cluster mostly in the TDF and CSF volcanic facies fields. The rock types of our samples plot mainly in the spinifex, orthocumulate and mesocumulate fields. These two factors discount the likelihood of DC and LLLS facies being present in the Fisher East komatiitic system (Fig. 14).

Characteristics of nickel sulfide mineralization

Nickel sulfide mineralization was intersected in drillholes MFED018, MFED001, MFED029, MFED043, MFED069 and MFED071 (Fig. 3), predominantly as Type-I basal contact massive sulfides (cf. Lesher and Keays, 2002; Table 3) with subordinate matrix sulfides. Sulfide veins or stringers are also present in komatiites at the Cannonball prospect (drillhole MFED069; Fig. 15a). Nickel sulfides appear to have been remobilized as a result of deformation but appear to have remained close to, or maintained, their original footwall position.

Massive and vein sulfides are also hosted by felsic metasedimentary rocks (drillhole MFED015) and shales (MFED016). The timing of sulfide accumulation is unclear, but could be syn- to post-magmatic, or potentially reflect remobilization of pre-existing ore zones. Sulfide compositions in these intersections include pentlandite, pyrrhotite, pyrite, violarite and minor amounts

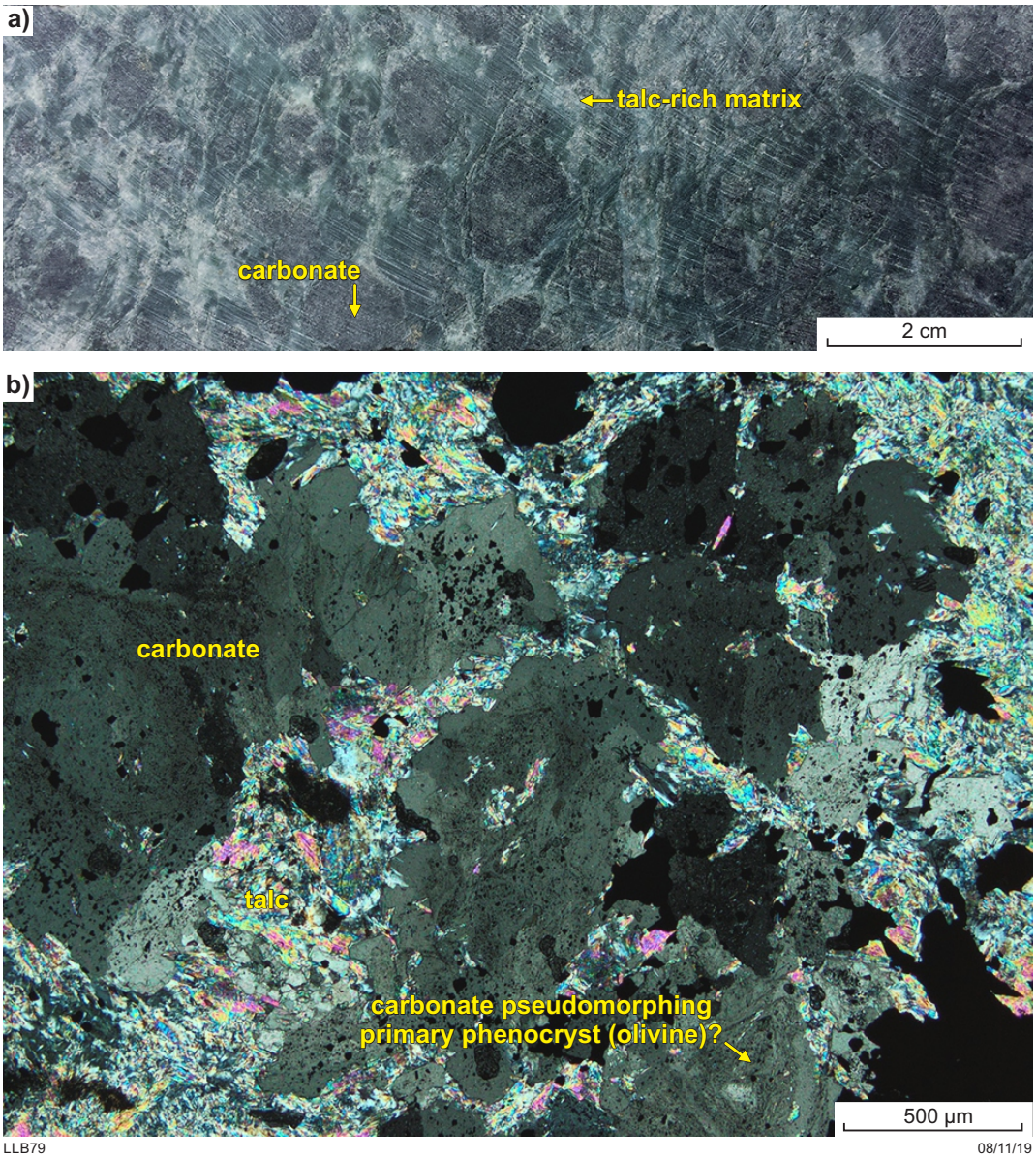

Figure 10. Photos of talc-rich komatiites: a) core photo from drillhole MFED069 ~250 m; b) thin section photo (under crossed polars) from drillhole MFED043 ~317 m

of chalcopyrite. Sulfides in drillhole MFED015 are intensely weathered, although element mapping using the TORNADO XRF suggests that Fe-rich sulfides are dominant (their magnetism suggests pyrrhotite; Fig. 16; Appendix 4). Element mapping of shale-hosted sulfides in drillhole MFED016 suggest the presence of pyrite and pentlandite (Appendix 4; GSWA sample 218721).

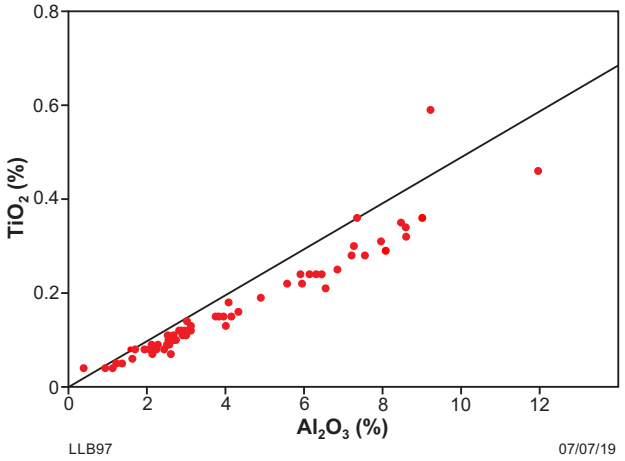

Figure 11. Al_2O_3/TiO_2 ratios of komatiites from Fisher East prospects. The chondritic mantle line from Barnes (2006) is also shown

Table 4. Geochemical characteristics of A- and B-Zone komatiites on the basis of whole-rock geochemistry. Unknown rock types were excluded from the calculations. A-zone, *n* = 30; B-zone, *n* = 36

	SiO_2 (wt%)	TiO_2 (wt%)	Al_2O_3 (wt%)	Fe_2O_3 (wt%)	MnO (wt%)	MgO (wt%)	CaO (wt%)	Na_2O (wt%)	K_2O (wt%)	P_2O_5 (wt%)	Ni (ppm)	Zr (ppm)	Cr (ppm)
Chlorite-rich (A-Zone) komatiites													
Average	48.31	0.24	6.06	0.57	0.15	29.43	6.68	0.08	0.06	0.024	1806.1	16.6	2642
Minimum	41.28	0.07	1.94	0.25	0.06	24.21	0.40	0.03	0.01	0.009	680.0	4.0	1098
Maximum	55.94	0.59	11.96	1.19	0.30	42.03	15.73	0.12	0.16	0.050	7347.9	54.0	5245
Standard deviation	3.50	0.11	2.42	0.30	0.06	3.29	3.79	0.02	0.07	0.009	1222.6	10.4	735
Talc-rich (B-Zone) komatiites													
Average	45.37	0.09	2.36	0.56	0.18	36.28	5.87	0.09	0.02	0.013	6397.9	8	2308
Minimum	37.10	0.04	0.39	0.03	0.04	25.72	0.11	0.06	X	0.004	1819.0	3	601
Maximum	56.66	0.18	4.08	1.94	0.53	48.76	16.41	0.13	0.03	0.027	30667.0	29	8668
Standard deviation	4.10	0.03	0.81	0.48	0.10	5.51	4.91	0.02	0.01	0.006	7063.1	5	1364

Discussion

Nickel potential of the Fisher East greenstone belt

Distribution of komatiite flow facies

The relatively high MgO concentrations in talc-rich zones at Fisher East prospects (29–49% MgO) indicate that they were probably originally B-Zones, representing cumulate-textured komatiites (Fig. 10). In contrast, the lower MgO concentrations for chlorite-rich komatiites (24–32% MgO) suggest that they were possibly finer grained pyroxene-rich zones, or likely spinifex-textured A-Zones (Fig. 9). The differences in the chemistry and mineralogy of these zones reflect different proportions of original cumulus olivine before talc–carbonate alteration. The Ni/Cr vs Ni/Ti ratio crossplot (Fig. 14) independently confirms the presence of both A- and B-Zones and is useful for further discriminating orthocumulate- and mesocumulate-textured komatiites in B-Zones. Olivine adcumulates, which elsewhere have been characterized by very low Al_2O_3 and TiO_2 contents and MgO contents >50 wt% (Hill et al., 1988), have not been observed at Fisher East. Olivine adcumulates are common in the Kalgoorlie Terrane, more so than in other terranes in the Yilgarn Craton (Barnes and Fiorentini, 2012).

Komatiites at Fisher East have Al_2O_3/TiO_2 ratios slightly higher (Al-undepleted to slightly Al-enriched; Fig. 11) than the Al-undepleted komatiites from the Kalgoorlie Terrane (e.g. Barnes, 2006) and those from Munro Township in the Superior Province, Canada, the type example of Al-undepleted komatiites (Ardnt et al., 1977; Nesbitt et al., 1979). These differences might reflect crustal contamination or post-depositional alteration, although the narrow range of Al_2O_3/TiO_2 ratios in the Fisher East samples rules out significant mobility of these elements; it is more likely an effect of minor differences in the komatiite source composition. Although the Al_2O_3/TiO_2 ratios in the Fisher East komatiite samples are not extreme (e.g. compared to those in the Commondale greenstone belt in South Africa; Wilson, 2003), they differ from those of typical komatiites previously documented in the EGST (e.g. Barnes, 2006). From a mineralization perspective, an assessment by Barnes and Fiorentini (2012) of various mineralized terranes around the world has found no relationship between mantle source characteristics and nickel endowment, so any komatiite, including Al-enriched types, has the potential to host significant nickel deposits if all of the critical ingredients for mineralization are present.

Crustal contamination of komatiites

Contamination of mantle-derived melts by crustal rocks during emplacement can be interpreted by comparing incompatible trace element ratios (Barnes, 2006). For example, high degrees of crustal assimilation are indicated by high TiO_2/Zr and La/Sm ratios, which is the case for some samples at Fisher East (Fig. 13). In the Sm vs La plot (Fig. 13b), about half of the data fall to the left of the assumed pristine mantle ratio line, suggesting that the source is weakly to moderately depleted. Physical

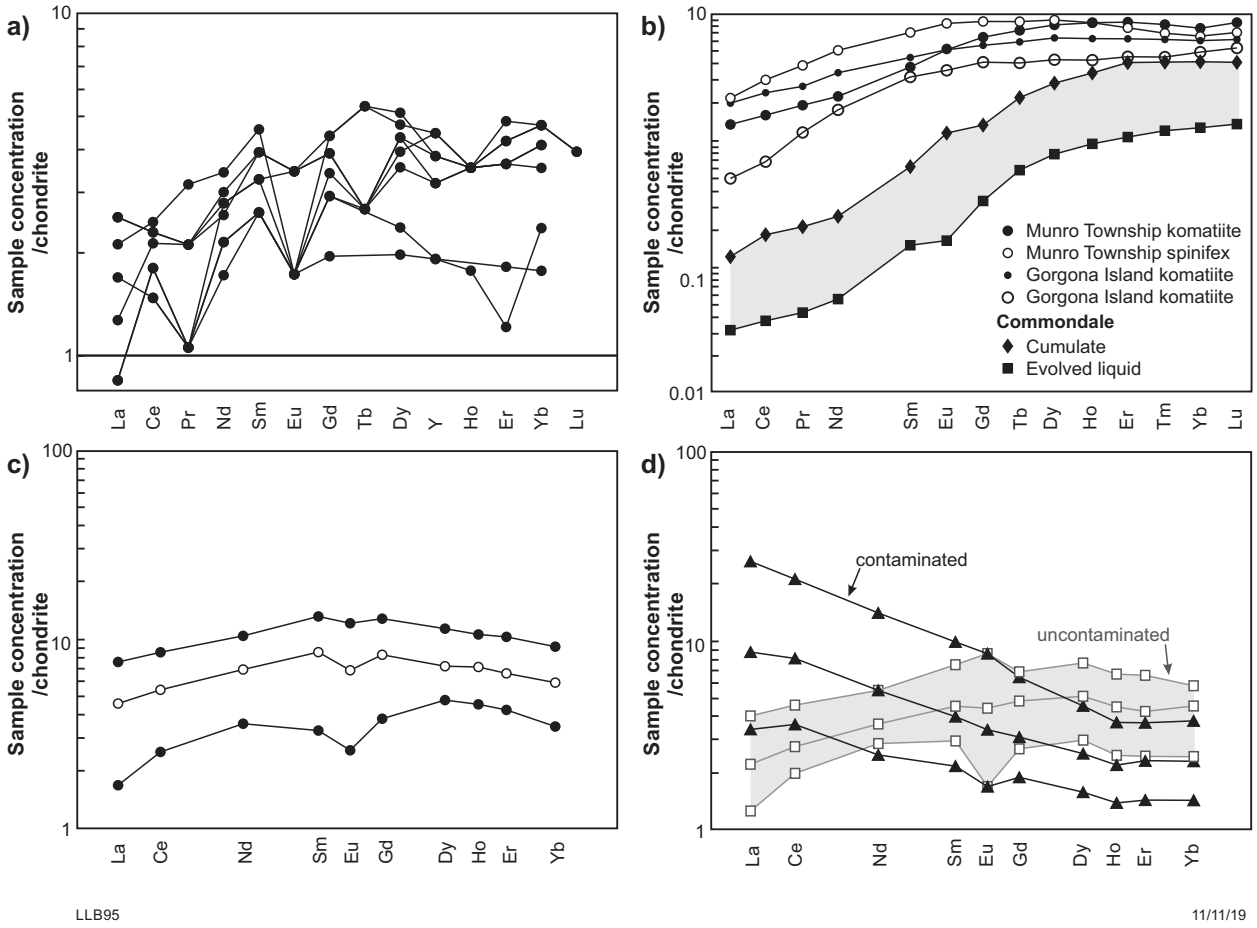

Figure 12. Comparison of REE patterns of komatiite samples from Fisher East with those of various other komatiites: a) selected komatiite samples from Fisher East (GSWA samples 218601, 218797, 218795, 218763, 218768, 218755, 218782 and 218774; for details of samples see Appendix 4). Highly altered or contaminated samples and those with >2% SO_3 were excluded. Chondrite-normalized according to Sun and McDonough (1989); b) komatiite data (Wilson, 2003) from Commondale (South Africa; Al-enriched), Munro (Canada; Al-undepleted) and Gorgona Island (off Colombia; high Al_2O_3/TiO_2 ratios; Arndt et al., 2008). Chondrite-normalized according to Sun and McDonough (1989); c) uncontaminated Al-depleted and d) contaminated (specifically from the Black Swan area, Yilgarn Craton) and uncontaminated (shaded grey) Al-undepleted komatiites; compilations of data from the Abitibi and Norseman–Wiluna greenstone belts (from Barnes, 2006; chondrite-normalized according to McDonough and Sun, 1995)

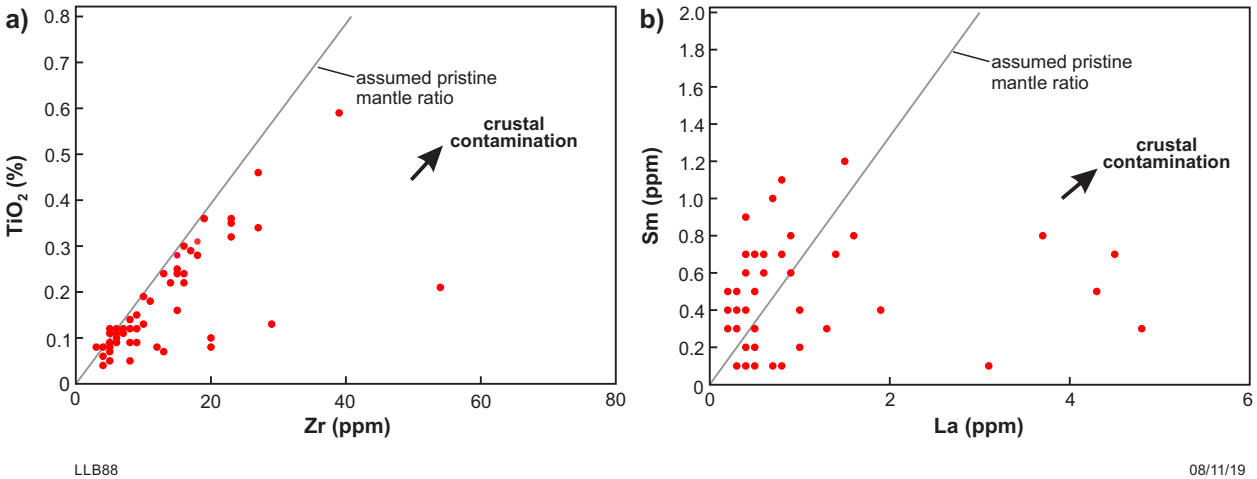

Figure 13. Selected ratios of incompatible trace elements for komatiites from Fisher East: a) TiO_2 vs Zr; b) Sm vs La. The grey line represents the assumed pristine mantle ratio for each element pair (normalizing values after McDonough and Sun, 1995); data trends that deviate from this line in the direction of the 'crustal contamination' arrows likely represent crustal contamination (adapted from Barnes, 2006)

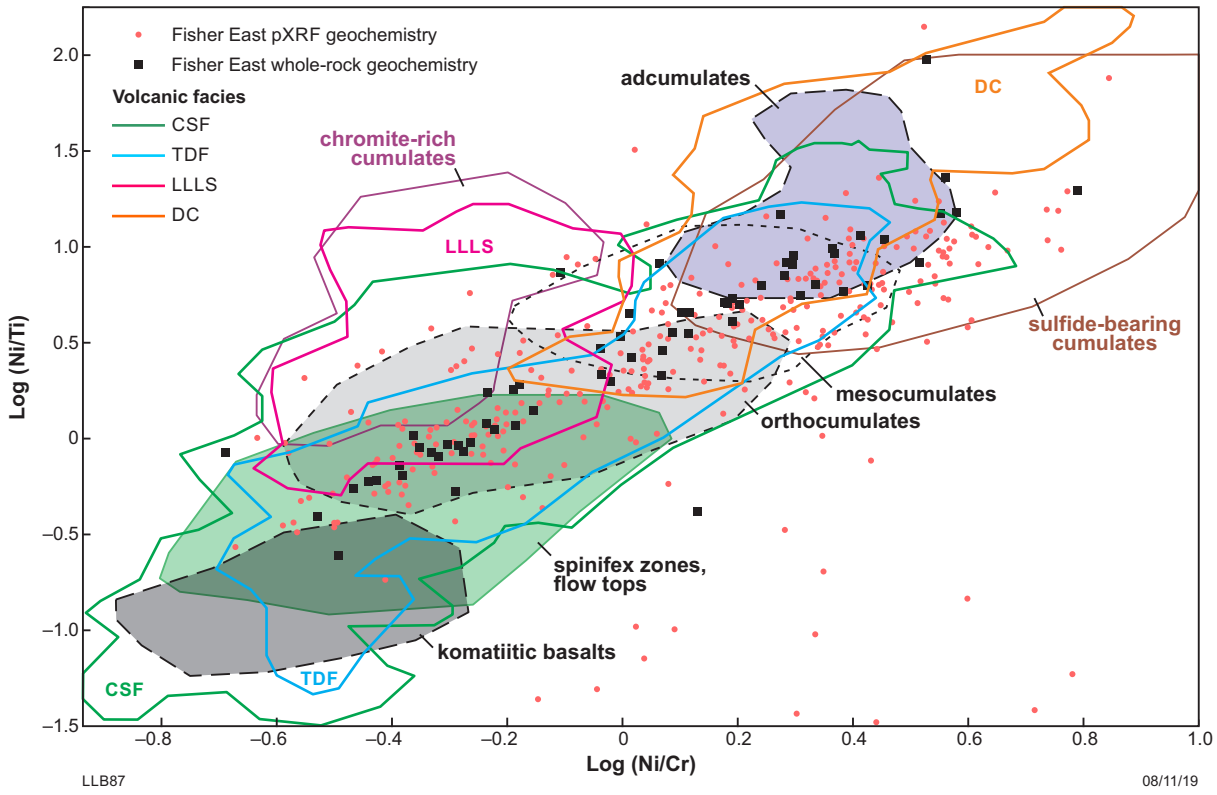

Figure 14. Ni/Cr vs Ni/Ti ratios from whole-rock and pXRF data from Fisher East samples overlaid on fields representing volcanic facies (Barnes et al., 2004) and rock types (Le Vaillant et al., 2016). The volcanic facies fields enclose 80% of data points from Barnes and Fiorentini (2012) for thin differentiated flows (TDF), channelized sheet flows (CSF – Kambalda style), dunitic channelized flows (DC) and layered lava lakes or sills (LLLS)

evidence for crustal contamination at Fisher East includes the incorporation of rafts of felsic metasedimentary footwall rocks within massive sulfides (Fig. 5). Crustal contamination is important in nickel mineralizing systems as it indicates assimilation of sulfur-rich sediments and continental crust, which can lead to sulfur saturation of melts and accumulation of nickel sulfides (Lesher et al., 2001; Barnes et al., 2004). Comparative studies in the Yilgarn Craton by Barnes and Fiorentini (2012) suggest that crustal contamination in the Kalgoorlie Terrane is more intense and spatially more extensive than in any other terrane in the EGST.

Volcanogenic setting and mineralization

A schematic flow field model has been created for the Fisher East prospects, based on the stratigraphy and differentiation of A- and B-Zones (Fig. 17). The stratigraphic footwall contact of the komatiite has been used as the horizontal datum in order to depict variations in thickness between flows. This contact was used as it was clearly identified in all cores studied. This model does not account for topographic changes (including erosion of the footwall by komatiites) or structural complexity. Basal contacts between komatiites and felsic volcanic and volcaniclastic sedimentary rocks show signs of cross-contact assimilation (Figs 5–7), whereas the hangingwall contacts do not. Where hangingwall contacts are preserved, they are interpreted to be primary conformable stratigraphic or structural contacts. Thus, the komatiites are interpreted here as flows rather than intrusions, although more work is needed to fully understand the nature of the contacts.

The Fisher East prospects exhibit Type I mineralization, as documented by Lesher and Keays (2002), and it is restricted to localities with thick B-Zones, such as Camelwood and Musket. These localities are interpreted to be high-energy lava channels (e.g. Hill, 2001; Barnes, 2006). Lava channels are typically associated with large volumes of magma, continued magma flow-through with minimal heat loss, and both strong thermomechanical erosion of underlying rocks and chemical modification of the magma are common (Lesher et al., 1984; Lesher, 1989; Hill, 2001; Barnes, 2006). It can be inferred from our geochemical data and drillcore observations that the komatiites that host mineralization at Fisher East are channelized sheet flows (Fig. 14) that are comparable to the type example of mineralized komatiites at Kambalda in the Kalgoorlie Terrane (Lesher et al., 1984).

Footwall characteristics

Mineralization at Fisher East is broadly comparable to the style of mineralization at Kambalda in the Kalgoorlie Terrane. The source of sulfur at Fisher East is unknown, and BIF is absent in all the significantly mineralized drillholes at Camelwood (MFED018, MFED001, MFED029), Cannonball (MFED069) and Musket (MFED043), where the primary footwall rocks are felsic volcanic and volcaniclastic metasedimentary rocks.

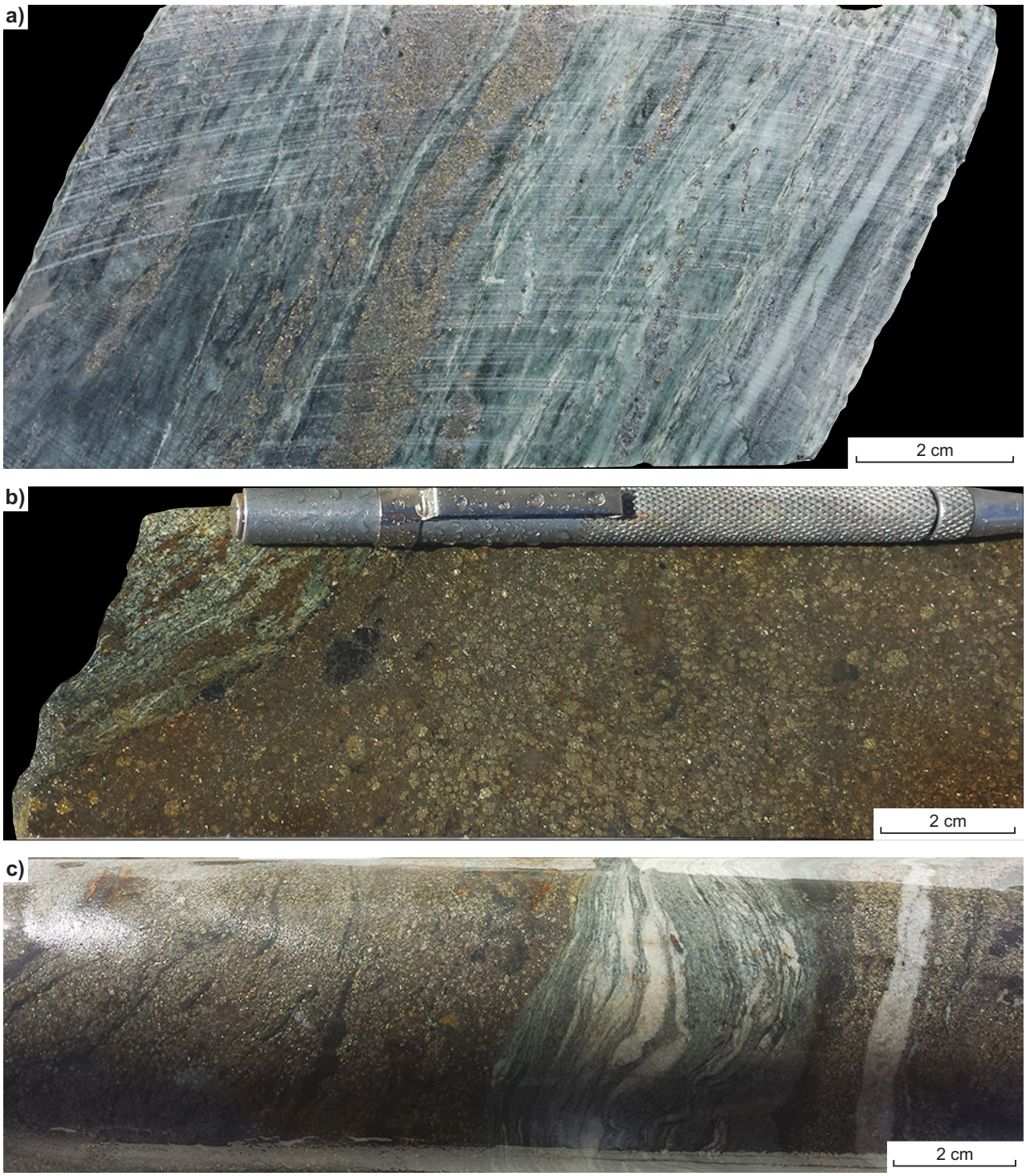

Figure 15. Core photos showing styles of mineralization at the Fisher East prospects: a) sulfide veins in drillhole MFED069, Cannonball prospect; b) massive sulfides in drillhole MFED043 (305 m), Musket prospect; c) massive sulfides with intermittent komatiites in drillhole MFED018 (416 m), Camelwood prospect

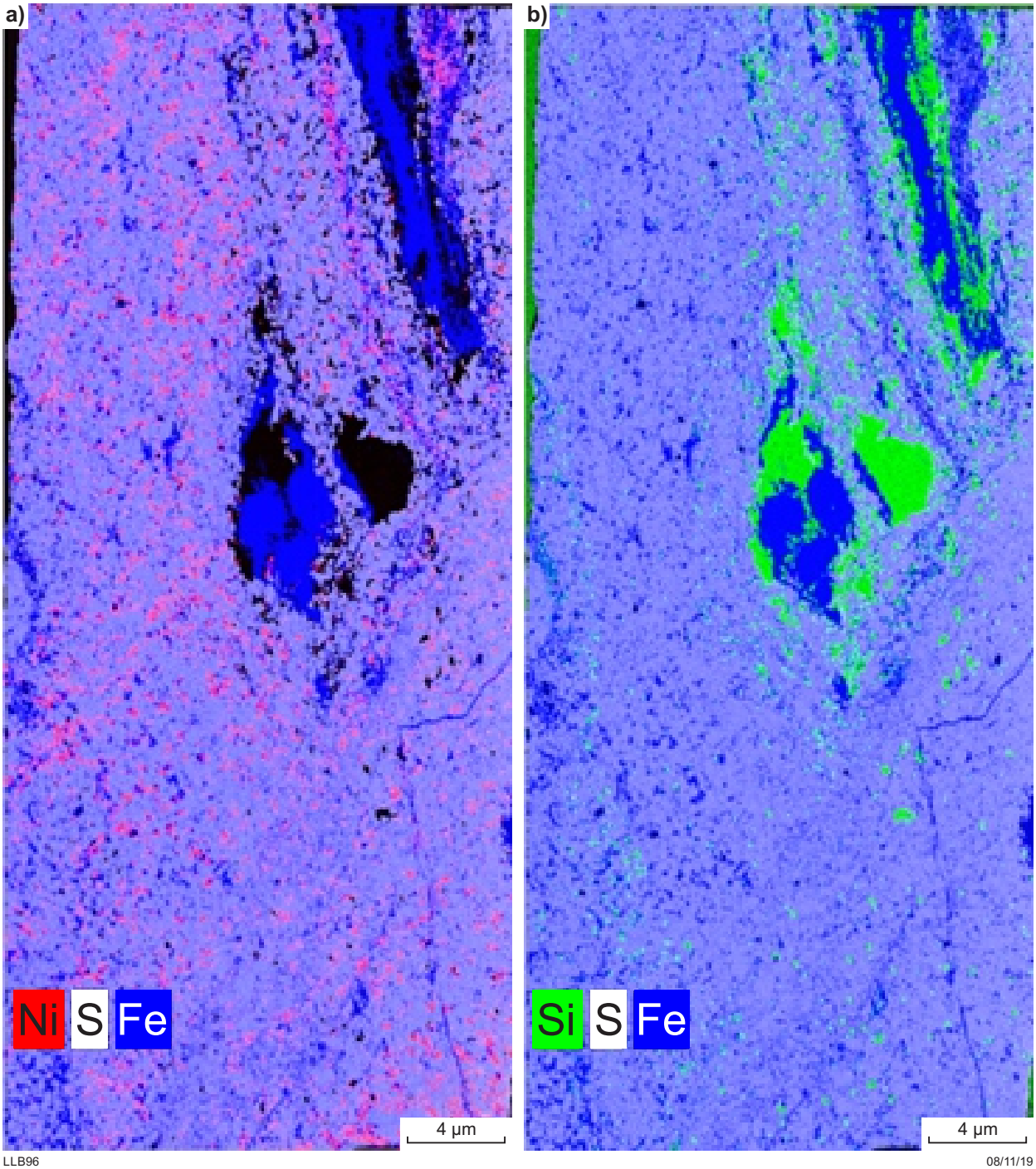

Figure 16. Bruker TORNADO XRF images of intensely weathered sulfides in drillhole MFED015 (202.65 m) with false colours highlighting: a) Ni, S and Fe; b) Si, S and Fe

However, BIF units are present within komatiite sequences, along with footwall felsic volcanic and volcaniclastic metasedimentary rocks, in the less-mineralized drillholes flanking the mineralized areas. Where contacts between these BIF units and komatiite are present, there are examples of BIF fragmentation and inclusion within the komatiite, or ductile deformation of BIF units (Fig. 18). Thus, some interaction between BIF and magma appears likely, possibly involving thermomechanical erosion of footwall units including BIF. Rox Resources Limited (2015) reported the presence of (?exhalative) sulfides in BIF in areas distal to the Fisher East komatiites. Although this relationship does not provide definitive evidence of assimilation of sulfur from underlying BIF leading to sulfur saturation in ultramafic magmas at the site of present nickel mineralization, it does support the interpretation that the addition of sulfur may have been by assimilation of sulfur-rich footwall units somewhere along the flow path of the ultramafic magmas.

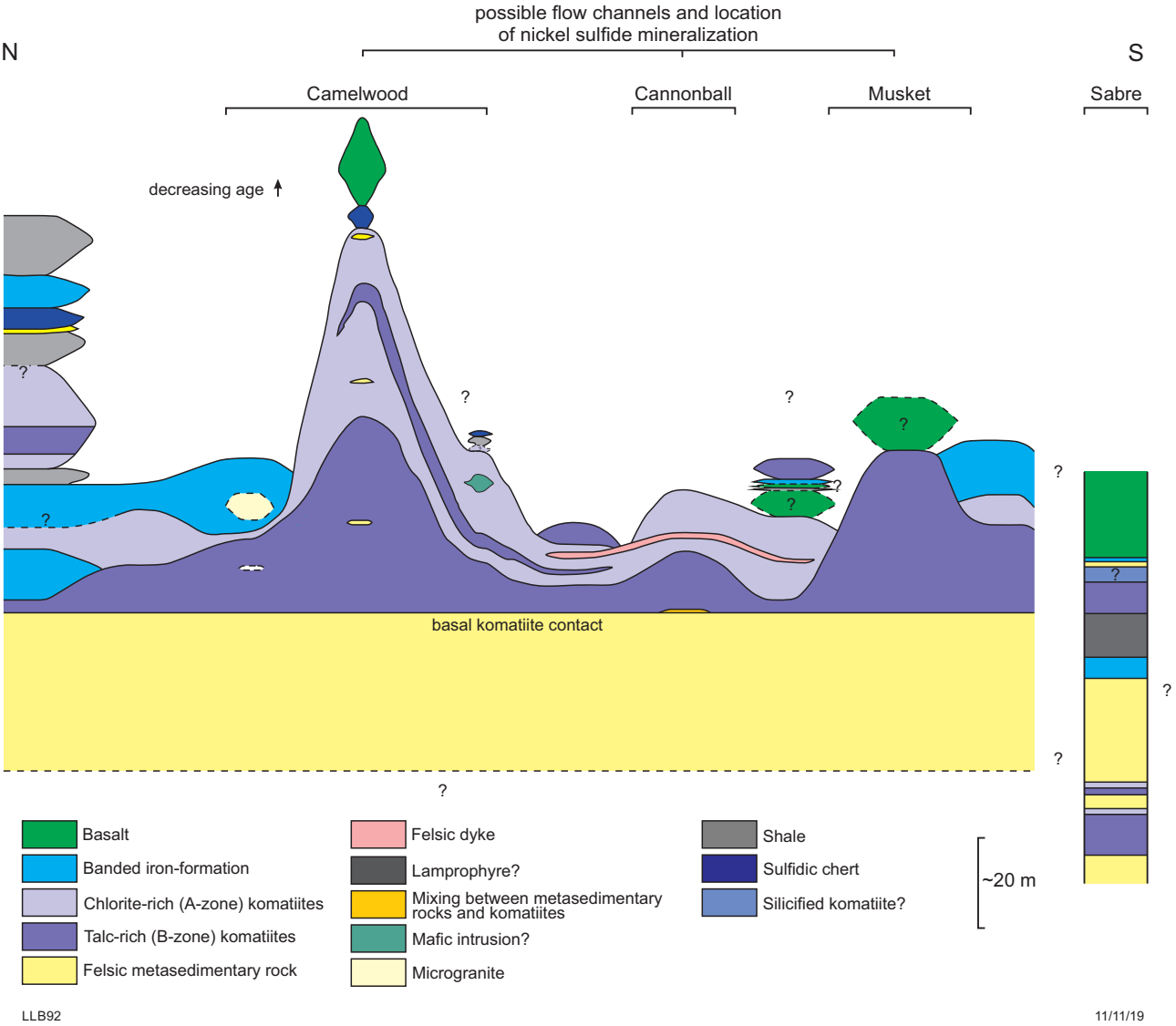

Figure 17. Interpretive flow-field model of Fisher East based on core logging, geochemistry and lithological contacts. The model is better constrained in the north where there are more drillholes (see Fig. 2). The single drillhole at the Sabre prospect is ~7 km south of the other prospects and is therefore separated from the rest of the model. Note that this model is not at true horizontal scale and the vertical scale is greatly exaggerated. The datum for the basal komatiite contact (black line) is 0 m above sea level. This model does not consider topographic changes or structural complexity

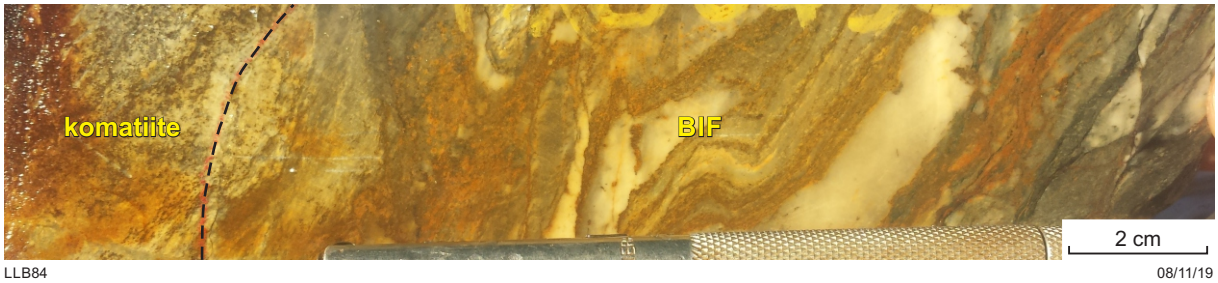

Figure 18. Core photo showing ductile deformation of BIF in contact with komatiite. Rough location of contact outlined. Drillhole MFED016 ~211 m

Conclusions

The komatiites at Fisher East represent a type of komatiite that has not previously been documented in the EGST, although their age and stratigraphic associations are broadly comparable to the komatiites of the Youanmi Terrane (e.g. Forrestania). The results of this study suggest that the Fisher East area, and large areas of the adjoining Kurnalpi and Burtville Terranes, are prospective for economic discoveries of komatiite-hosted nickel sulfides, despite subtle differences of the komatiites there from the heavily Ni-endowed komatiites of the Kalgoorlie Terrane. The komatiites at Fisher East host several massive and net-textured nickel sulfide occurrences at their basal contacts, demonstrating that they have several of the prerequisites for hosting large nickel sulfide deposits. Firstly, proxies for crustal contamination indicate that the Fisher East komatiites locally assimilated evolved crust or sediments, which is necessary for komatiitic liquids to attain the sulfur saturations required to crystallize sulfide minerals. Secondly, the thick intervals of high-Mg olivine cumulates at Fisher East are interpreted to represent extremely hot and turbulent lava flow channels. Thirdly, lavas from such channels are rich in nickel, which is also a prerequisite for crystallization of nickel sulfides. These features are important when considering prospectivity at greenstone belt scale and are characteristics of world-class nickel deposits in the Kalgoorlie Terrane, such as at Perseverance (Barnes and Fiorentini, 2012).

Further study of the Fisher East greenstone belt is needed to determine the style of komatiite emplacement (intrusive or extrusive), to evaluate the extent of structural mobilization of massive sulfides, and to examine geophysical and geochemical gradients surrounding the Fisher East prospects. Such studies will assist future research into the prospectivity of the greenstone belts in the neighbouring Kurnalpi and Burtville Terranes.

Acknowledgements

This Report is underpinned by research conducted by Lauren Burley for her Master of Ore Deposit Geology at The University of Western Australia, which was supported by the Geological Survey of Western Australia. We thank Rox Resources for providing access to drillcore and other data and for logistical support during the project. Drs Marco Fiorentini, Steve Barnes (co-author of this Report) and David Mole are thanked for their supervision of Lauren's research and for their guidance and support throughout the project. Thanks also to Dr Margaux Le Vaillant for providing advice about the collection and calibration of pXRF data.

References

Arndt, N, Lesher, CM and Barnes, SJ 2008, Komatiite: Cambridge University Press, New York, 467p.

Arndt, NT, Naldrett, AJ and Pyke, DR 1977, Komatiitic and iron-rich tholeiitic lavas of Munro Township, northeast Ontario: Journal of Petrology, v. 18, p. 319–369.

Barley, ME, Eisenlohr, B, Groves, DI, Perring, CS and Vearncombe, JR 1989, Late Archaean convergent margin tectonics and gold mineralization: a new look at the Norseman-Wiluna Belt: Geology, v. 17, p. 826–829.

Barnes, SJ (editor) 2006, Nickel deposits of the Yilgarn Craton: geology, geochemistry, and geophysics applied to exploration: Society of Economic Geologists, 210p.

Barnes, SJ 2013, Lithogeochemistry applied to exploration for magmatic Ni-Cu-PGE ore deposits: Advances in Exploration and Ore Deposit Geochemistry, p. 1–2.

Barnes, SJ and Fiorentini, ML 2012, Komatiite magmas and nickel sulphide deposits: a comparison of variably endowed Archean terranes: Economic Geology, v. 107, p. 755–780.

Barnes, SJ, Hill, RET, Perring, CS and Dowling, SE 2004, Lithogeochemical exploration of komatiite-associated Ni-sulphide deposits: strategies and limitations: Mineralogy and Petrology, v. 82, p. 259–293.

Barnes, SJ, Van Kranendonk, MJ and Sonntag, I 2012, Geochemistry and tectonic setting of basalts from the Eastern Goldfields Superterrane: Australian Journal of Earth Sciences, v. 59, p. 707–735.

Barnes, SJ and Van Kranendonk, MJ 2014, Archean andesites in the east Yilgarn craton, Australia: Products of plume-crust interaction?: Lithosphere, v. 6, no. 2, p. 80–92.

Begg, GC, Griffin, WL, O'Reilly, SY and Natapov, LM 2010, Archean cratonic architecture: implications for the Yilgarn and Superior Provinces, *in* Yilgarn–Superior Workshop — Abstracts, Fifth International Archean Symposium, 10 September 2010: Geological Survey of Western Australia, Record 2010/20, p. 1–3.

Berman, M, Bischof, L and Huntington, J 1999, Algorithms and software for the automated identification of minerals using field spectra or hyperspectral imagery, *in* Proceedings of the 13th International Conference on Applied Geologic Remote Sensing: Vancouver, British Columbia, Canada, 1 March 1999, p. 222–232.

Bruker Corporation 2015, M4 Tornado: Brunker Corporation, viewed 19 October 2015, <www.bruker.com/products/x-ray-diffraction-and-elemental-analysis/micro-xrf-and-txrf/m4-tornado/technical-details.html>.

Burley, LL, Barnes, SJ, Laukamp, C, Mole, DR, Le Vaillant, M and Fiorentini, ML 2017, Rapid mineralogical and geochemical characterisation of the Fisher East nickel sulphide prospects, Western Australia, using hyperspectral and pXRF data: Ore Geology Reviews, v. 90, p. 371–387.

Cassidy, KF, Champion, DC, Krapez, B, Barley, ME, Brown, SJA, Blewett, RS, Groenewald, PB and Tyler, IM 2006, A revised geological framework for the Yilgarn Craton, Western Australia: Geological Survey of Western Australia, Record 2006/8, 8p.

Cudahy, T, Jones, M, Thomas, M, Laukamp, C, Caccetta, M, Hewson, R, Rodger, A and Verrall, M 2008, Next generation mineral mapping: Queensland airborne HyMap and satellite ASTER surveys 2006–2008: CSIRO, Exploration and Mining Report P2007/364, 152p.

Czarnota, K, Blewett, RS and Goscombe, B 2008, Structural and metamorphic controls on gold through time and space in the central Eastern Goldfields Superterrane – a field guide: Geological Survey of Western Australia, Record 2008/9, 66p.

Czarnota, K, Champion, DC, Goscombe, B, Blewett, RS, Cassidy, KF, Henson, PA and Groenewald, PB 2010, Geodynamics of the eastern Yilgarn Craton: Precambrian Research, v. 183, p. 175–202.

Geological Survey of Western Australia 2009, Compilation of geochronology information, 2009: Geological Survey of Western Australia, digital data package.

Gole, MJ, Barnes, SJ and Hill, RET 1987, The role of fluids in the metamorphism of komatiites, Agnew nickel deposit, Western Australia: Contributions to Mineralogy and Petrology, v. 96, p. 151–162.

Gole, MJ and Hill, RET 1990, The refinement of extrusive models for the genesis of nickel deposits: implications from case studies at Honeymoon Well and the Walter Williams Formation: Minerals and Energy Research Institute of Western Australia, Report 68, 93p.

Hancock, EA, Green, AA, Huntington, JF, Schodlok, MC and Whitbourn, LB 2013, HyLogger-3: implications of adding thermal-infrared sensing: Geological Survey of Western Australia, Record 2013/3, 24p.

Hancock, EA and Huntington, JF 2010, The GSWA NVCL HyLogger: Rapid mineralogical analysis for characterizing mineral and petroleum core: Geological Survey of Western Australia, Record 2010/17, 21p.

Herzberg, C, Condie, K and Korenaga, J 2010, Thermal history of the earth and its petrological expression: Earth and Planetary Science Letters, v. 292 (1–2), p. 79–88.

Hill, RET 2001, Komatiite volcanology, volcanological setting and primary geochemical properties of komatiite-associated nickel deposits: Geochemistry: Exploration, Environment, Analysis, v. 1, p. 365–381.

Hill, RET, Barnes, SJ, Gole, MJ and Dowling, SE 1995, The volcanology of komatiites as deduced from field relationships in the Norseman-Wiluna greenstone belt, Western Australia: Lithos, v. 34, p. 159–188.

Hill, RET, Gole, MJ and Barnes, SJ 1988, Physical volcanology of komatiites: Geological Society of Australia, Excursion Guide Book No. 1, 74p.

Hoatson, DM, Jaireth, S and Jaques, AL 2006, Nickel sulphide deposits in Australia: Ore Geology Reviews, v. 29, p. 177–241.

Hronsky, JMA and Schodde, RC 2006, Nickel exploration history of the Yilgarn Craton, *in* Nickel deposits of the Yilgarn Craton: Geology, Geochemistry, and Geophysics Applied to Exploration: Society of Economic Geologists, Special Publication 13, p. 1–11.

Huntington, JF, Mason, P and Berman, M 1997, Geological evaluation of The Spectral Assistant (TSA) for mineralogical interpretation: CSIRO, Exploration and Mining Report 417R, 86p.

Korsch, RJ, Kositcin, N and Champion, DC 2011, Australian island arcs through time: geodynamic implications for the Archean and Proterozoic: Gondwana Research, v. 19, p. 716–734.

Kositcin, N, Brown, SJA, Barley, ME, Krapez, B, Cassidy, KF and Champion, DC 2008, SHRIMP U-Pb zircon age constraints on the Late Archaean tectonostratigraphic architecture of the Eastern Goldfields Superterrane, Yilgarn Craton, Western Australia: Precambrian Research, v. 161, p. 5–33.

Krapez, B and Barley, MEB 2008, Late Archaean synorogenic basins of the Eastern Goldfields Superterrane, Yilgarn Craton, Western Australia: Part III. Signatures of tectonic escape in the arc-continent collision zone: Precambrian Research, v. 161, p. 183–199.

Laukamp, C, Caccetta, M, Chia, J, Cudahy, T, Gessner, K, Haest, M, Liu, YC, Ong, C and Rodger, A 2010, The uses, abuses and opportunites for hyperspectral technologies and derived geoscience information, *in* Extended abstracts: Geo-Computing 2010, Australian Institute of Geoscientists; Brisbane, Australia, September 2010, AIG Bulletin No. 51, p. 73–76.

Laukamp, C, Termin, KA, Pejcic, B, Haest, M and Cudahy, T 2012, Vibrational spectroscopy of calcic amphiboles – application for exploration and mining: European Journal of Mineralogy, v. 24, p. 863–878.

Le Vaillant, M, Barnes, SJ, Fisher, L, Fiorentini, ML and Caruso, S 2014, Use and calibration of portable X-Ray fluorescence analysers: application to lithogeochemical exploration for komatiite-hosted nickel sulphide deposits: Geochemistry: Exploration, Environment, Analysis, v. 14, p. 199–209.

Le Vaillant, M, Fiorentini, ML and Barnes, SJ 2016, Review of lithogeochemical exploration tools for komatiite-hosted Ni-Cu-(PGE) deposits: Journal of Geochemical Exploration, v. 168, p. 1–19.

Lesher, CM 1989, Komatiite-associated nickel sulfide deposits, *in* Ore deposition associated with magmas *edited by* JA Whitney, AJ Naldrett and JM Robertson: Reviews in Economic Geology, v. 4, p. 44–101.

Lesher, CM, Arndt, NT and Groves, DI 1984, Genesis of komatiite-associated nickel sulphide deposits at Kambalda, Western Australia: a distal volcanic model, *in* Sulphide deposits in mafic and ultramafic rocks *edited by* DL Buchanan and MJ Jones: The Institution of Mining and Metallurgy, London, p. 70–80.

Lesher, CM, Burnham, OM, Keays, RR, Barnes, SJ and Hulbert, L 2001, Trace-element geochemistry and petrogenesis of barren and ore-associated komatiites: The Canadian Mineralogist, v. 39, p. 673–696.

Lesher, CM and Keays, RR 2002, Komatiite-associated Ni-Cu-(PGE) deposits: Geology, mineralogy, geochemistry, and genesis, *in* The geology, geochemistry, mineralogy, and mineral benefication of the Platinum-Group Elements *edited by* LJ Cabri: Canadian Institute of Mining, Metallurgy and Petroleum, Montreal, Special Volume 54, p. 579–617.

Martin, D McB, Johnson, SP and Riganti, A 2016, 1:500 000 State interpreted bedrock geology of Western Australia, Extracted from GeoVIEW.WA: Geological Survey of Western Australia.

Martin, D McB, Johnson, SP and Riganti, A 2017, 1:500 000 tectonic units of Western Australia, Extracted from GeoVIEW.WA: Geological Survey of Western Australia.

McDonough, WF and Sun, SS 1995, The composition of the Earth: Chemical Geology, v. 120, p. 223–253.

Miller, JM 2010, Laverton Region, *in* Controls on giant mineral systems in the Yilgarn Craton – a field guide *compiled by* TC McCuaig, JM Miller and S Beresford: Geological Survey of Western Australia, Record 2010/26, p. 45–67.

Mole, DR, Burley, L and Barnes, SJ 2016, A new komatiite-hosted Ni–Cu–PGE event in the Eastern Goldfields Superterrane, *in* 13th international Ni–Cu–PGE symposium, Fremantle, Australia: Abstracts *edited by* B Godel, S Barnes, I Gonzales-Alvarez, M Fiorentini and M Le Vaillant: Geological Survey of Western Australia, Record 2016/13, p. 57.

Nelson, DR 1997, Evolution of the Archaean granite-greenstone terranes of the Eastern Goldfields, Western Australia: SHRIMP U-Pb zircon constraints: Precambrain Research, v. 83, p. 57–81.

Nesbitt, RW, Sun, S-S and Purvis, AC 1979, Komatiites: geochemistry and genesis: Canadian Mineralogist, v. 17, p. 165–186.

Pawley, MJ, Romano, SS, Hall, CE, Wyche, S and Wingate, MTD 2009, The Yamarna shear zone: a new terrane boundary in the northeastern Yilgarn Craton?: Geological Survey of Western Australia Annual Review 2007–08: Geological Survey of Western Australia, p. 27–32.

Perring, CS, Barnes, SJ and Hill, RET 1996, Geochemistry of komatiites from Forrestania, Southern Cross Province, Western Australia: evidence for crustal contamination: Lithos, v. 37, p. 181–197.

Pyke, DR, Naldrett, AJ and Eckstrand, RO 1973, Archaean ultramafic flows in Munro Township, Ontario: Geological Society of America Bulletin, v. 84, p. 955–978.

Rox Resources Limited 2015, Nickel sulphide discovery confirmed at Sabre prospect: Report to Australian Securities Exchange, 13 May 2015.

Rox Resources Limited 2019, Rox commences drilling at Mt Fisher gold project: Report to Australian Securities Exchange, 11 June 2019.

Said, N, Kerrich, R, Cassidy, K and Champion, DC 2012, Characteristics and geodynamic setting of the 2.7 Ga Yilgarn heterogeneous plume and its interaction with continental lithosphere: evidence from komatiitic basalt and basalt geochemistry of the Eastern Goldfields Superterrane: Australian Journal of Earth Sciences, v. 59, p. 737–763.

Schumulian, ML 1984, Windarra nickel deposits, Western Australia, *in* Sulphide deposits in mafic and ultramafic rocks *edited by* DL Buchanan and MJ Jones: The Institution of Mining and Metallurgy, London, p. 95–102.

Sonntag, I, Laukamp, C and Hagemann, SG 2012, Low potassium hydrothermal alteration in low sulfidation epithermal systems as detected by IRS and XRD: An example from the Ca-O miner, Eastern Mindanao, Philippines: Ore Geology Reviews, v. 45, p. 47–60.

Sproule, RA, Lesher, CM, Ayer, JA, Thurston, PC and Herzberg, CT 2002, Spatial and temporal variations in the geochemistry of komatiites and komatiitic basalts in the Abitibi greenstone belt: Precambrian Research, v. 115, p. 153–186.

Standing, JG 2008, Terrane amalgamation in the Eastern Goldfields Superterrane, Yilgarn Craton: evidence from tectonostratigraphic studies of the Laverton greenstone belt: Precambrian Research, v. 161, p. 114–134.

Sun, S-S and McDonough, WF 1989, Chemical and isotopic systematics of oceanic basalt: Implications for mantle composition and processes *in* Magmatism in the ocean basins *edited by* AD Saunders and MJ Norry: Geological Society, London, Special Publication 42, p. 313–345.

Swager, CP 1997, Tectono-stratigraphy of late Archaean greenstone terranes in the southern Eastern Goldfields, Western Australia: Precambrian Research, v. 83, p. 11–42.

Swager, CP, Witt, WK, Griffin, TJ, Ahmat, AL, Hunter, WM, McGoldrick, PJ and Wyche, S 1992, Late Archaean granite–greenstones of the Kalgoorlie Terrane, Yilgarn Craton, Western Australia, *in* The Archean: Terrains, processes and metallogeny *edited by* JE Glover and SE Ho: Geology Department, Key Centre and University Extension, The University of Western Australia; Third International Archaean Symposium, Perth, Western Australia, 17 September 1990, Publication 22, p. 107–122.

Wager, LR, Brown, GM and Wadsworth, WJ 1960, Types of igneous cumulates: Journal of Petrology, v. 1, p. 73–85.

Wilson, AH 2003, A new class of silica enriched, highly depleted komatiites in the southern Kapvaal Craton, South Africa: Precambrian Research, v. 127, p. 125–141.

Witt, WK, Cassidy, KF, Lu, Y and Hagemann, SG 2018, The tectonic setting and evolution of the 2.7 Ga Kalgoorlie-Kurnalpi Rift, a world-class Archean gold province: Mineralium Deposita, doi:10.1007/s00126-017-0778-9.

This Report documents the results of volcanological and mineralogical studies conducted in the Mount Fisher greenstone belt, and compares these characteristics to other greenstone belts that host nickel sulfide mineralization in the Yilgarn Craton. Despite the komatiites being extensively deformed, field relationships and the use of geochemical and hyperspectral data can help reconstruct original rock types, the environment in which the komatiites erupted, and proxies for mineralization. Although Fisher East komatiites are broadly more comparable to those of the Youanmi Terrane in terms of lithostratigraphy and age, they share similar characteristics with the Kalgoorlie Terrane komatiites when it comes to proxies for mineralization, and have the key ingredients necessary to form nickel sulfide mineralization.

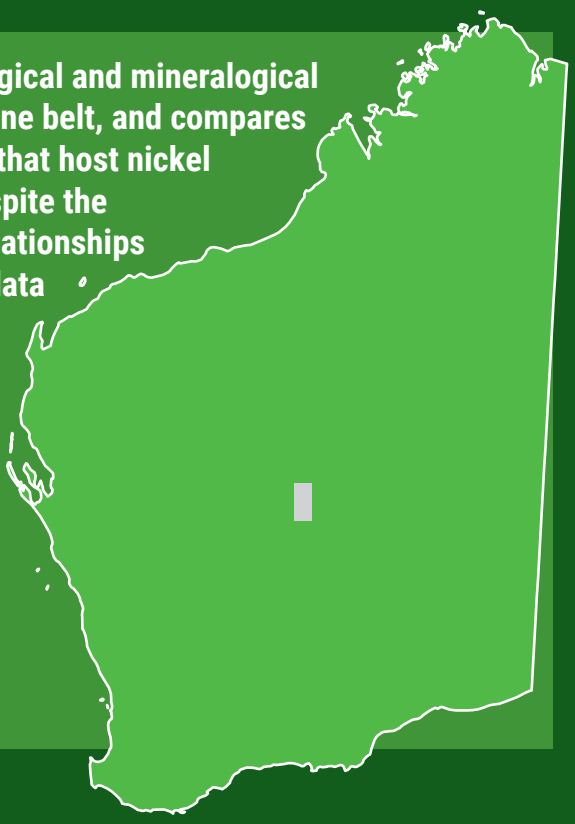

BURLEY AND BARNES

KOMATIITE CHARACTERISTICS OF THE FISHER EAST NICKEL SULFIDE PROSPECTS: IMPLICATIONS FOR NICKEL PROSPECTIVITY IN THE NORTHEASTERN YILGARN CRATON

REPORT 198

Further details of geoscience products are available from:

Information Centre
Department of Mines, Industry Regulation and Safety
100 Plain Street
EAST PERTH WA 6004
Phone: (08) 9222 3459 Fax: (08) 9222 3444

www.dmp.wa.gov.au/GSWApublications